5-26-2017 12:00 AM

Degradation of Glass Fiber Reinforced Polyamide 6 Composites Throughout the Direct Long-Fiber Reinforced Thermoplastic Process

Thomas Whitfield
The University of Western Ontario

Supervisor
Dr. Takashi Kuboki
The University of Western Ontario

Graduate Program in Mechanical and Materials Engineering
A thesis submitted in partial fulfillment of the requirements for the degree in Master of Engineering Science

Abstract

The direct long-fiber reinforced thermoplastic (D-LFT) process is a streamlined material processing technique which includes various types of equipment. It is imperative to understand how the process and its operating conditions affect degradation and thermal properties of the processed material for industry applications. This study investigates effects of process stages, extruder temperature, and screw speed on molecular weight and thermal properties of glass fiber reinforced polyamide 6 (PA6) composites throughout the D-LFT process. Viscosity number (VN) measurements, thermogravimetric analyses (TGA) and differential scanning calorimetry (DSC) analyses were performed on collected samples. In conclusion, it was found that thermo-oxidative degradation is the main degradation mechanism of the glass fiber reinforced PA6 composites during the D-LFT process. Therefore, minimizing temperature and residence time of the extruders as well as exposure time of plastificate to atmospheric conditions along the conveyer is an effective way to minimize degradation of PA6.

Keywords

Polyamides, Glass Fibers, Composites, Processing, D-LFT, Thermal Properties

Co-Authorship Statement

1.

Title: Thermal Properties of Glass Fiber Reinforced Polyamide 6 Composites throughout the Direct Long-Fiber Reinforced Thermoplastic Process (Chapter 2)

Authors: **Thomas Whitfield**[1], Takashi Kuboki[1], Jeffrey Wood[1], Vanja Ugresic[2], Shyam Sathyanarayana[3], and Koffi Dagnon[4]

1. Department of Mechanical and Materials Engineering, University of Western Ontario, London, Ontario, Canada, N6A 5B9
2. Fraunhofer Project Centre for Composites Research, University of Western Ontario, London, Ontario, Canada, N6M 0E1
3. BASF Corporation, Wyandotte, Michigan, USA, 48192
4. BASF Corporation, Budd Lake, New Jersey, USA, 07828

Thomas Whitfield collected, analyzed, and interpreted the data under the constructive suggestions of Dr. Takashi Kuboki. Thomas Whitfield drafted the manuscript under the guidance of Dr. Takashi Kuboki, and the manuscript was revised by Dr. Takashi Kuboki and Dr. Jeffrey Wood. Manufacturing of the composites was conducted by Vanja Ugresic. The viscosity number experiments were performed by Dr. Shyam Sathyanarayana and Dr. Koffi Dagnon. The manuscript was accepted by Polymer Engineering & Science.

2.

Title: Effects of Process Parameters on Thermal Properties of Glass Fiber Reinforced Polyamide 6 Composites throughout the Direct Long-Fiber Reinforced Thermoplastics Process (Chapter 3)

Authors: **Thomas Whitfield**[1], Takashi Kuboki[1], Jeffrey Wood[1], Vanja Ugresic[2], Shyam Sathyanarayana[3], and Koffi Dagnon[4]

1. Department of Mechanical and Materials Engineering, University of Western Ontario, London, Ontario, Canada, N6A 5B9
2. Fraunhofer Project Centre for Composites Research, University of Western Ontario, London, Ontario, Canada, N6M 0E1
3. BASF Corporation, Wyandotte, Michigan, USA, 48192
4. BASF Corporation, Budd Lake, New Jersey, USA, 07828

Thomas Whitfield collected, analyzed, and interpreted the data under the constructive suggestions of Dr. Takashi Kuboki. Thomas Whitfield drafted the manuscript under the guidance of Dr. Takashi Kuboki, and the manuscript was revised by Dr. Takashi Kuboki and Dr. Jeffrey Wood. Manufacturing of the composites was conducted by Vanja Ugresic. The viscosity number experiments were performed by Dr. Shyam Sathyanarayana and Dr. Koffi Dagnon. The manuscript will be submitted for publication.

Acknowledgments

First and foremost, I would like to express my greatest gratitude to my supervisor Dr. Takashi Kuboki for giving me this valuable opportunity to continue my studies at Western University. His guidance, patience and constructive suggestions throughout my master study not only helped me to gain understanding but also taught me strong work ethics and the required attitude for research.

Much appreciation would be expressed to my co-supervisor Dr. Jeff Wood and to Dr. Ying Fan for their support and contributions to this work. I am also grateful to Dr. Xueliang Sun, Dr. Robert Klassen, and Dr. Andrew Hrymak for being my examiners. My thanks to Vanja Ugresic and the staff of the Fraunhofer Project Center for Composites Research at the University of Western Ontario, as well as Dr. Shyam Sathyanarayana and Dr. Koffi Dagnon at BASF Corporation for their technical support. I would also like to thank the faculty and staff members in the Department of Mechanical and Materials Engineering at the University of Western Ontario for all their assistance. I would like to thank Dr. Paul Charpentier for allowing me to access his laboratory facility to perform characterization tests used in this research.

I am also grateful for the financial support provided by Automotive Partnership Canada (APC), BASF Corporation, ElringKlinger Canada Inc., Dieffenbacher North America, General Motors of Canada Company (GM), and Johns Manville.

Finally, I would like to express my grateful thanks to my family for their unending love and support and to my friends for their help and encouragement.

Table of Contents

List of Tables

List of Figures

Chapter 1

1 Introduction

Fiber reinforced polymer is a light material which has good mechanical properties and is one of the most versatile materials available to engineers today [1]. Since their introduction to industry markets in the 1960s, fiber reinforced polymers have been utilized in various industries, such as transportation, sporting goods, construction, and more [2]. The wide adoption of this material is a result of its ability to be tailored to meet specific requirements, which can be achieved through selections of materials and process techniques. For many years, the transportation industry, such as the aerospace and automotive industries, has been replacing high-density materials with fiber reinforced polymers.

There are two types of polymers: thermoplastics and thermosets. The resin type determines what process techniques can be utilized. A thermoset is created when liquid resin is converted into a hard rigid solid by cross-linking, which leads to formation of a tightly bound three-dimensional network [3]. The cross-linking process is irreversible and is performed typically after fibers are incorporated into liquid resin. The most commonly used thermosets are epoxy, unsaturated polyester and vinyl ester. A thermoplastic, unlike a thermoset, is not cross-linked but rather derives its strength from long molecules which provide molecular entanglements [3]. The melt-solidification process of a thermoplastic is reversible through heating, which causes disentanglement and a change from a rigid solid to a viscous liquid [3]. The most commonly used thermoplastics are polyethylene and

polypropylene. The automotive industry has been utilizing both fiber reinforced thermosets and thermoplastics in various applications. Fiber-reinforced thermoplastics are typically chosen for parts requiring a high level of production and short cycle times while fiber-reinforced thermosets are commonly employed for those requiring high mechanical properties or higher service temperatures. It has been more common for the automotive industry to use fiber reinforced thermosets [4]. However, a long-fiber reinforced thermoplastic (LFT), which has high mechanical property, is increasingly used due to advancement of their processing techniques.

1.1 Processing techniques for long-fiber reinforced thermoplastics

Typically, a composite which has an average fiber length greater than 2 mm is considered to be a long-fiber reinforced thermoplastic (LFT) [5]. Process techniques of long-fiber reinforced thermoplastics can be divided into two categories: indirect process and direct process.

1.1.1 Indirect process

Indirect process utilizes semi-finished products, which are made by mixing all the ingredients in a step that is separate from the molding operation.

A glass mat thermoplastic (GMT) is a semi-finished sheet that was developed at the end of the 1960s [5]. GMT can be either a continuous woven mat or long fibers (>12.5 – 100 mm) imbedded in a thermoplastic matrix [5]. One of the processes to manufacture GMT is the molding impregnation in double band presses, in which a thermoplastic is first melted via an extruder and ejected between two continuous rolls of fiber mats and

consolidated in a double belt press. GMT is cut to a required size, which is predetermined by the final shape of the part, and is then heated and compressed in a mold by a press. Advantage of this process is that a final product has a homogeneous fiber distribution. However, since GMT is a semi-finished product, molding operation must be done in a separate stage, which increases matrix degradation as well as process time and cost [6]. Also, GMT has restricted in-mold flow capabilities due to the fact that the tightly woven fiber mat prevents the fibers from flowing during compression, thus requiring the GMT size to be close to the final size of the part [5].

The long-fiber reinforced thermoplastic granulate (LFT-G) is another type of a semi-finished product. The semi-finished product in this technique is long-fiber reinforced thermoplastic pellets, which can then be processed in injection molding, injection compression molding, or extrusion compression molding [6]. Long-fiber reinforced thermoplastic pellets are prepared by wirecoating, crosshead extrusion, or several pultrusion techniques [5]. This process allows us to manufacture a final product with complex geometry. The major drawback of this process technique is fiber breakage during molding operation. The fiber length is originally constrained by the length of the pellets and further decreased by a screw in a plastification unit of a molding machine [5].

1.1.2 Direct process

The direct long-fiber reinforced thermoplastic (D-LFT) process incorporates multiple process stages into a single production line, removing the need for semi-finished products. The D-LFT process, depicted in Figure 1.1, is a one-stop manufacturing process starting from raw materials to a final product, and includes various types of equipment.

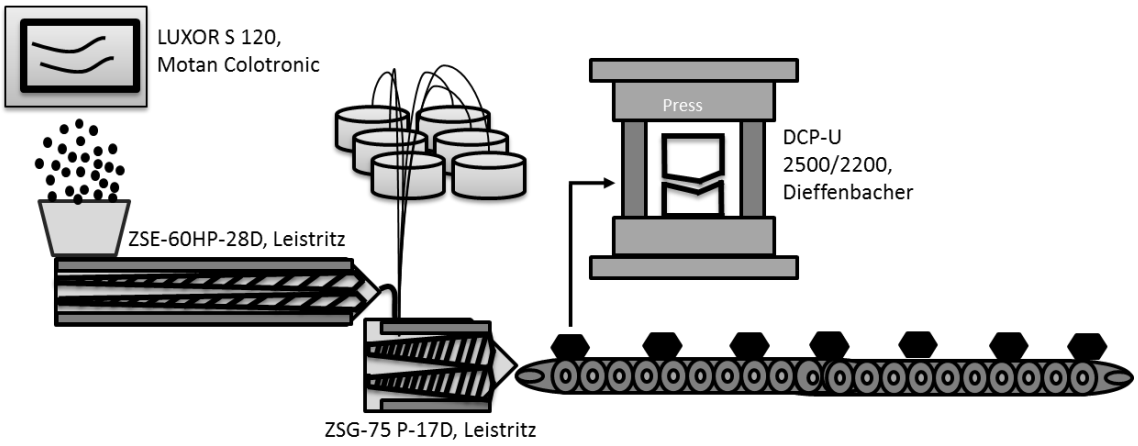

Figure 1.1 Schematic of D-LFT process with identified equipment.

The process is summarized as follows: dried polymer pellets, along with any required additives (such as heat stabilizers, flame retardants, colorants, etc.), are gravimetrically fed into the first twin-screw extruder to be blended. A film die, which is attached to the end of the first extruder, transfers the blended, molten plastic into the second extruder. The plastic is briefly introduced to atmospheric conditions at a molten state as it flows from the film die into the second extruder. The molten plastic is then combined with continuous fibers in the second extruder, which are pulled directly into the extruder from continuous bobbins. The glass fiber strands are wrapped around the screws within the second extruder and are broken down into appropriate fiber lengths, typically 5-50mm [6]. The plastificate, which is the molten LFT charge that is formed in the second extruder, is ejected onto the conveyor where it is cut into an appropriate shot size using a shear cutter. Finally, the plastificate is transferred to a compression molding machine to shape and solidify the plastificate into the final part.

Since the initial development of the D-LFT process, the optimal operating conditions have been an area of study [5] and LFTs have continued to be introduced to new

applications, such as in the automotive industry [7]. Although the D-LFT process removes the separate processing of semi-finished products, the energy intensive processes that are used in the direct process of LFTs can influence material properties of the product. It is, therefore, advantageous to select polymer matrix that is not highly susceptible to energy intensive process, as doing so allows for a larger process window. Polypropylene (PP) has been widely used as a polymer matrix in the D-LFT process because of its good processability, its ability to be tailored for specific applications, and its retention of mechanical properties after recycling [8] as well as its low melting temperature. PP is a highly crystalline polymer that leads to greater stiffness, tensile strength, modulus and hardness [9]. However, PP does not have as good mechanical and thermal properties as engineering plastics. Polyamide 6 (PA6) is a good candidate as a polymer matrix in the D-LFT process because it has high toughness over a large range of temperature, good impact and abrasion resistance, lubricity, and resistance to organic solvents [10]. PA6 has a range of possible applications, including those requiring thermal stability, fire resistance, and good mechanical properties [10]. Despite its mechanical performance, PA6 can be limited by its susceptibility to degradation [10][11][12][13][14][15].

1.2 Background

1.2.1 Effects of Process Conditions of Extruder on Properties of Fiber Reinforced Thermoplastics

As mentioned above, the D-LFT process includes tandem twin-screw extruders (i.e., the first and second extruders), which are the main components of the D-LFT process. There has been extensive study into the effect of extruder process conditions on the produced materials [16][17]. Stade [18] was the first to discuss the basic concepts and approaches

for the production of a glass fiber reinforced thermoplastics. It was stated that one of the most basic requirements for the compounding of fiber reinforced thermoplastics is the limitation and control of the thermal degradation of the base polymer, which is a resultant of the energy imposed on the polymer. This study was an important establishment in research and provided insight into how the properties of fiber reinforced thermoplastics are dependent on process techniques used. Stade showed that the energy imposed on the polymer from the process is dependent on the polymer's melt viscosity and can be influenced by the temperature within the extruder. From this study, further research into the effect of temperature and other process conditions on properties of fiber reinforced thermoplastics has continued.

Important process parameters for the optimization of an extrusion process are the screw speed and barrel temperature of the extruder [17][19]. These two parameters have an influence on material properties of the product as shown below.

1.2.1.1 Screw Speed

Capone et al. [20] studied thermal and mechanical degradation of polystyrene (PS) and Poly(methyl methacrylate) (PMMA) during extrusion. The results showed that the increase of screw speed reduced loss in molecular weight of the polymers, which was considered to possibly be a result of the shortened residence time in the extruder and the reduction in shear stress on the polymer due to the wall slip phenomena. Yilmazer and Cansever [21] presented a study on the influence of process conditions on fiber length in the extrusion and subsequent injection molding process using glass fiber reinforced PA6. It was shown

that when the shear rate (i.e., screw speed and/or feed rate) inside the twin-screw extruder was increased, the average fiber length was decreased.

1.2.1.2 Extruder Temperature

Popescu et al. [22] used mathematical and experimental techniques to predict the mechanical properties of glass fiber reinforced polyamide 6.6 when processed under different extruder temperatures (a polyamide resin similar to PA6). This study shows that the extruder temperature can have an influence on the physical properties of the final product. Salleh et al. [23] investigated the effect of extruder temperature on the rheological, dynamic mechanical and tensile properties of kenaf fiber reinforced high density polyethylene (HDPE). It was found that high extruder temperature resulted in increased complex viscosity, storage and loss modulus and improved tensile modulus of extruded composites. Kelly et al. [24] showed that, for a single screw extruder, the screw geometry can have a significant effect on the melt temperature profile of the polymer in the extruder. Also, Vera-Sorroche et al. [25] discussed the importance of melt homogeneity on polymer quality and studied how it is influenced by screw geometry, screw rotation speed and set temperature. It was found that each of these screw conditions has a significant effect on the thermal homogeneity of polymer melt within the extruder, which affects the quality of the polymer produced.

1.2.2 Properties of Polyamide 6

The effects of variation in processing conditions on fiber length and fiber distribution in the PA matrix have been one of the main research interests because fiber length and fiber distribution affect the mechanical properties of fiber reinforced PA6 composites [21].

However, it is also important to study the effects of process condition on properties of the PA6 matrix such as molecular weight, thermal decomposition, and crystallization; the next section reviews these properties.

1.2.2.1 Molecular Weight of Polyamide 6

Polymer degradation can occur through heat, shear, oxidation, or a combination of the three mechanisms. These degradation mechanisms influence the molecular structure of a polymer primarily though breaking of bonds in the main polymer chain [26]. Chain scission and cross-linking occur in polyamides during a composite process and affect their molecular weight [10][27][28][29]. The competition between chain scission and cross-linking dictates decrease [29], increase [30], and their combination [31][32] of molecular weight of polyamides.

Lozano-González et al. [30] injection-molded PA6 repeatedly over a range of 10 cycles. Results from gel permeation chromatography (GPC) showed that molecular weight of the PA6 was increased with each reprocess cycle and postulated that the recombination of broken chains was the dominant reaction. However, Su et al. [32] injection-molded PA6 repetitively over a range of 16 cycles. GPC results showed that a reduction in the molecular weight and an increase in the molecular weight distribution, and they suggested that chain scission was the predominant reaction. Crespo et al. [33] and Lee et al. [34] also reported that melt viscosity of PA6 decreased with increasing process cycles in the repeated injection molding and repeated extrusion, respectively.

1.2.2.2 Thermal Decomposition of Polyamide 6

Beyler and Hirschler [26] raised the importance of a distinction between thermal degradation and thermal decomposition and used the definition of the American Society for Testing Materials (ASTM). Thermal decomposition is the "process whereby the action of heat or elevated temperature on an item causes change to the chemical composition" [35]. Thermal degradation is the "process whereby the action of heat or elevated temperature on a material or assembly causes an adverse change in one or more properties" [35]. The difference between these two phenomena is important to this current study because one of its objectives is to quantify the degradation of a material sample through analysis of the decomposition profile.

In almost all cases, heat must be supplied to a material for it to reach a temperature where adverse changes to the material's properties occur, such as a loss of physical, mechanical, or electrical properties, otherwise known as a point where thermal degradation ensues [35]. A material's ability to resist these changes despite elevated temperatures is a measure of its thermal stability. Also, due to heating or elevated temperatures, it is possible for chemical species changes to begin to occur, otherwise known as thermal decomposition [35]. The decomposition process may either generate (exothermic) or utilize (endothermic) additional heat [26]. The magnitude of this energy generation or energy requirement, which is subject to change as decomposition continues, can be measured by differential thermal analyses (DTA) [26]. The amount of energy either absorbed or given off is dependent on the chemical composition of the material and the decomposition mechanisms [26]. Activation energy is a measurement of the material's energy production or usage of energy during decomposition.

Decomposition of solid material is a complex process in which the relationship between mass loss and time is established as the result of varying degrees, and is affected by both sample properties and measurement conditions [36]. The use of thermogravimetric analysis (TGA) to determine thermal stability and decomposition behavior has attracted much attention [37][38][39]. However, the kinetics parameters, such as activation energy, are highly dependent on the experimental conditions and mathematical treatment used for evaluation [40]. As a result, there has been much comparison of, and discussion about the accuracy of, and mathematical models for decomposition kinetics [40][41][42][43]. Despite differences that arise between experimental conditions and mathematical treatment, activation energy has still been widely used in experimental studies to describe decomposition kinetics. Scully and Bissessur [44] used activation energy to determine the graphite filler content in PA6 that produced the greatest enhancement to thermal stability. In a similar study, Pashaei et al. [45] used activation energy to determine changes in the thermal stability of PA6 after inclusion of glass fibers compared with nanocomposites. Not only has activation energy been used to assess the effect of additives on decomposition kinetics, but also the effect of process and post-process conditions. Zou et al. [46] used two mathematical models (Kissinger and Ozawa) comparatively to determine the effect of thermo-oxidative degradation on activation energy in long glass-fiber reinforced PA6. Their study found that the Ozawa method was more suitable for supplying reliable information with their experimental conditions and found that the thermo-oxidative degradation modified the flammability and decomposition behavior of the reinforced composites.

Another method for the determination of activation energy is the Ozawa/Flynn and Wall method, which is described in ASTM E1641-15 [47] and is the method used in this study. The purpose of this experiment is to follow the procedures used in previous research to analyze how the thermal stability of PA6 changes throughout the process. It was expected that the thermal stability would decrease during the process as the material more easily decomposed due to the increased degradation of the molecular structure.

1.2.2.3 Crystallization of Polyamide 6

As a semi-crystalline polymer, PA6 has a structural network that is highly dependent on process conditions and thermal treatment [48]. The crystalline and amorphous regions of the PA6 structure have a complete and mostly-complete satisfaction of hydrogen bonds, respectively [49]. The configuration of the crystalline region can adopt one of two phases: the α-phase and the γ-phase. The α-phase has polymer chains fully extended and oriented in an anti-parallel fashion. The alternative phase, the γ-phase, has polymer chains twisted at an angle of approximately 60° in order to maintain complete satisfaction of hydrogen bonds. Kyotani and Mitsuhashi [50] showed that the formation of these phases is dependent on the crystallization temperature and time as well as annealing prior to analysis. At low crystallization temperatures, e.g. below 130°C, the γ-phase was the dominating phase, between 66% and 78%, but continuously decreased as the crystallization temperature increased and was lowered to 20% at 150°C. The shift between the two phases caused by change in the crystallization temperature is referred to as the Brill Transition and was first observed in polyamide 6,6 [51]. This occurrence was explained by the rate of formation of the γ-phase being greater than that of the α-phase at a crystallization temperature below

130°C, and vice versa for temperatures above 150°C. The rate of formation of the two phases was determined to be approximately equal within the range of 130°C to 150°C.

Processing affects crystal morphology and crystallization kinetics of PA6. Fornes and Paul [52] showed that γ-phase formation dominates in situations of rapid cooling, polymer chain mobility restriction, and/or high strain during crystallization. They concluded that only the γ-phase crystal structure was present in the skin of their injection molded parts, given conditions being favorable for its formation. In contrast, both the α-phase and the γ-phase were found in the core region of their injection-molded nanocomposite. The molding conditions that formulated these regions are similar to the conditions seen in compression molding.

Understanding crystalline phases is important because, ultimately, they affect the experimental crystallinity of the material. One impact of the two phases can often be captured during a non-isothermal DSC scan in the form of a small shoulder during the endothermic peak of melting. This shoulder has been observed in the past [53] and is a result of the difference in melting temperature between the two phases [54].

Fornes and Paul [52] also showed that extruded material showed faster crystallization than virgin material regardless of initial molecular weight. Several reasons for this finding were discussed; namely, impurities incorporated during extrusion created nucleation sites, and/or memory effects imposed upon the polymer during extrusion remained during thermal analysis. It has also been shown that process parameters, such as the melting temperature and time at a molten state, also influence crystallization of PA6 in a number of ways [55].

1.3 Objectives

The main objective of this study is to characterize properties of the PA6 matrix of glass fiber reinforced PA6 through the D-LFT process. Specific work includes:

(1) Characterizing molecular weight and thermal properties of the PA6 matrix of glass fiber reinforced PA6 at consecutive process stages within the D-LFT process.

(2) Investigating effect of process conditions within the D-LFT process on molecular weight and thermal properties of glass fiber reinforced PA6.

1.4 Significance

The D-LFT process is an emerging technology and offers a streamlined material processing technique and decreases the degradation of the material. To ensure product consistency and process optimization, it is imperative to understand how the process sequence and process conditions affect degradation and thermal properties of PA6, which is more susceptible to degradation than PP, during the D-LFT process. To the best of our knowledge, this is the first study to report how properties of polymer matrix changes at consecutive process stages and under different process conditions. The research outcome will assist equipment manufacturers in designing the D-LFT process for glass fiber reinforced PA6 composite products, as well as plastic manufacturers in developing PA6 tailored to the D-LFT process.

1.5 Thesis Outline

This thesis is prepared in an Integrated-Article format as specified by the School of Graduate and Postdoctoral Studies at Western University, London, Ontario, Canada. This thesis consists of four chapters:

Chapter 1 presents an introduction to processing of polymer composites and the D-LFT process and discusses use of PA6 as a polymer matrix. Chapter 1 also presents literature review on the influence of process conditions on polymers and properties of PA6 that are characterized in this study.

In Chapter 2, the D-LFT process is reviewed in more detail and variation in molecular weight and thermal properties of the glass fiber reinforced PA6 composites is investigated throughout the D-LFT process. Viscosity number (VN) measurements, thermogravimetric analyses (TGA), and differential scanning calorimetry (DSC) analyses were performed on samples taken from different locations along the D-LFT process.

In Chapter 3, variation in molecular weight and thermal properties of the glass fiber reinforced PA6 composites is investigated throughout the D-LFT process when extruder temperature and screw speed of the tandem twin-screw extruders, which are the main components of the D-LFT process, are changed. VN measurements, TGA and DSC analyses are performed on samples taken from different locations along the D-LFT process.

Chapter 4 summarizes and concludes the thesis and provides some recommendations for future work.

References

[1] Häuptli A. Direct processing of long fibre reinforced thermoplastics: Selecting a feeding system. Plast Addit Compd 2003;5:36–9. doi:10.1016/S1464-391X(03)00536-1.

[2] Astrom T. Manufacturing of Polymer Composites. London, UK: Chapman & Hall;

1997.

[3] Hull D, Clyne TW. An Introduction to Composite Materials. 2nd ed. New York: Cambridge University Press; 1996.

[4] Mazumdar S. Composites Manufacturing: Materials, Product, and Process Engineering. New York: CRC Press, Inc.; 2002.

[5] Schemme M. LFT – development status and perspectives. Reinf Plast 2008;52:32–9. doi:10.1016/S0034-3617(08)70036-5.

[6] Henning F, Ernst H, Brüssel R, Co G, Geiger O, Krause W, et al. LFTs for automotive applications. Reinf Plast 2005;49:24–33. doi:10.1016/S0034-3617(05)00546-1.

[7] Markarian J. Long fibre reinforced thermoplastics continue growth in automotive. Plast Addit Compd 2007;9:20–3. doi:10.1016/S1464-391X(07)70025-9.

[8] Balow MJ. Growth of Polypropylene Usage as a Cost-Effective Replacement of Engineering Polymers. In: Karian HG, editor. Handb. Polypropyl. Polypropyl. Compos., Basel, New York: Marcel Dekker, Inc.; 1999, p. 1–15.

[9] Chanda M, Roy SK. Industrial Polymers, Specialty Polymers, and Their Applications. Boca Raton, U.S.: Taylor & Francis Group; 2008.

[10] Levchik SV, Weil ED, Lewin M. Thermal decomposition of aliphatic nylons. Polym Int 1999;48:532–57. doi:10.1002/(sici)1097-0126(199907)48:7<532::aid-pi214>3.0.co;2-r.

[11] Pedroso AG, Mei LHI, Agnelli JAM, Rosa DS. The influence of the drying process time on the final properties of recycled glass fiber reinforced polyamide 6. Polym Test 2002;21:229–32. doi:10.1016/S0142-9418(01)00074-5.

[12] Davis RD, Gilman JW, VanderHart DL. Processing degradation of polyamide 6/montmorillonite clay nanocomposites and clay organic modifier. Polym Degrad Stab 2003;79:111–21. doi:10.1016/S0141-3910(02)00263-X.

[13] Kohan MI. Nylon Plastics Handbook. New York: Hanser Publishers; 1995.

[14] Pielichowski K, Njuguna J. Thermal Degradation of Polymeric Materials. Rapra Technology Limited; 2005.

[15] Lehrle RS, Parsons IW, Rollinson M. Thermal degradation mechanisms of Nylon 6 deduced from kinetic studies by pyrolysis-g.c. Polym Degrad Stab 2000;67:21–33. doi:10.1016/S0141-3910(99)00112-3.

[16] Chung C. Fundementals of Polymers. Extrus. Polym. Theory Pract. 2nd ed., Cincinnati, Ohio: Hanser Publications; 2011, p. 55–175.

[17] Covas JA, Gaspar-Cunha A. Chapter 5 - Polymer Extrusion - Setting the Operating Conditions and Defining the Screw Geometry. 2011.

[18] Stade K. Techniques for Compounding Glass Fiber-Reinforced Thermoplastics. Poloymer Eng Sci 1977;17:50–7.

[19] Agassant JF, Avenas P, Sergent JP, Carreau PJ. Polymer Processing Principles and Modeling. New York, N.Y.: Hanser Publishers; 1991.

[20] Capone C, Di Landro L, Inzoli F, Penco M, Sartore L. Thermal and Mechanical Degradation During Polymer Extrusion Process. Polym Eng Sci 2007;47:1813–9. doi:10.1002/pen.

[21] Yilmazer U, Cansever M. Effects of processing conditions on the fiber length distribution and mechanical properties of glass fiber reinforced nylon-6. Polym Compos 2002;23:61–71. doi:10.1002/pc.10412.

[22] Popescu A, Hancu L, Bere P. Research Concerning the Optimum Extrusion Temperature for Reinforced Polyamide. Appl Mech Mater 2013;371:394–8. doi:10.4028/www.scientific.net/AMM.371.394.

[23] Salleh FM, Hassan A, Yahya R, Azzahari AD. Effects of extrusion temperature on the rheological, dynamic mechanical and tensile properties of kenaf fiber/HDPE composites. Compos Part B Eng 2014;58:259–66. doi:10.1016/j.compositesb.2013.10.068.

[24] Kelly AL, Brown EC, Coates PD. The Effect of Screw Geometry on Melt Temperature Profile in Single Screw Extrusion. Polym Eng Sci 2006:1706–14. doi:10.1002/pen.20657.

[25] Vera-Sorroche J, Kelly A, Brown E, Coates P, Karnachi N, Harkin-Jones E, et al. Thermal optimisation of polymer extrusion using in-process monitoring techniques. Appl Therm Eng 2013;53:405–13. doi:10.1016/j.applthermaleng.2012.04.013.

[26] Beyler CL, Hirschler MM. Thermal Decomposition of Polymers. SFPE Handb.

Fire Prot. Eng. 4th ed., Quincy, U.S.: National Fire Protection Association; 2008, p. 110–31.

[27] Walter KD, Johnson JF, Tanaka J. Chapter 5 Polymer Degradation and Its Measurement. Eng. Dielectr. Vol. IIB Electr. Prop. Solid Insul. Mater. Meas. Tech., ASTM International (ASTM); 1987, p. 313–439.

[28] Crosslinking T. Thermo-oxidative Crosslinking 1988;26:3409–13.

[29] Goitisolo I, Eguiazábal JI, Nazábal J. Effects of reprocessing on the structure and properties of polyamide 6 nanocomposites. Polym Degrad Stab 2008;93:1747–52. doi:10.1016/j.polymdegradstab.2008.07.030.

[30] Lozano-González MJ, Rodriguez-Hernandez MT, Gonzalez-De Los Santos EA, Villalpando-Olmos J. Physical–mechanical properties and morphological study on nylon-6 recycling by injection molding. J Appl Polym Sci 2000;76:851–8. doi:10.1002/(SICI)1097-4628(20000509)76:6<851::AID-APP11>3.0.CO;2-D.

[31] Russo GM, Nicolais V, Di Maio L, Montesano S, Incarnato L. Rheological and mechanical properties of nylon 6 nanocomposites submitted to reprocessing with single and twin screw extruders. Polym Degrad Stab 2007;92:1925–33. doi:10.1016/j.polymdegradstab.2007.06.010.

[32] Su K-H, Lin J-H, Lin C-C. Influence of reprocessing on the mechanical properties and structure of polyamide 6. J Mater Process Technol 2007;192–193:532–8. doi:10.1016/j.jmatprotec.2007.04.056.

[33] Sengupta R, Chakraborty S, Bandyopadhyay S, Dasgupta S, Mukhopadhyay R, Auddy K, et al. Study of Rheological, Thermal, and Mechanical Behavior of Reprocessed Polyamide 6. Engineering 2007;47:21–5. doi:10.1002/pen.

[34] Lee KH, Lim SJ, Kim WN. Rheological and thermal properties of polyamide 6 and polyamide 6/glass fiber composite with repeated extrusion. Macromol Res 2014;22:624–31. doi:10.1007/s13233-014-2086-x.

[35] Materials B, Fires D, Smoke V, Properties FS, Assemblies MUF, Release VS, et al. Fire Standards 1 2013:1–26. doi:10.1520/E0176-12.2.

[36] Zakrzewski R. Pytolysis Kinetics of wood Comparison of Iso- and Polythermal Thermogravimetric Methods. Electron J Polish Agric Univ 2003;6.

[37] Cai Z, Mei S, Lu Y, He Y, Pi P, Cheng J, et al. Thermal properties and crystallite morphology of nylon 66 modified with a novel biphenyl aromatic liquid crystalline epoxy resin. Int J Mol Sci 2013;14:20682–91. doi:10.3390/ijms141020682.

[38] Sengupta R, Sabharwal S, Bhowmick AK, Chaki TK. Thermogravimetric studies on Polyamide-6,6 modified by electron beam irradiation and by nanofillers. Polym Degrad Stab 2006;91:1311–8. doi:10.1016/j.polymdegradstab.2005.08.012.

[39] Li J, Tong L, Fang Z, Gu A, Xu Z. Thermal degradation behavior of multi-walled carbon nanotubes/polyamide 6 composites. Polym Degrad Stab 2006;91:2046–52. doi:10.1016/j.polymdegradstab.2006.02.001.

[40] Chang TC, Shen WS, Chiu YS, Ho SY. Thermo-oxidative degradation of

phosphorus-containing polyurethane. Polym Degrad Stab 1995;49:353–60. doi:10.1016/0141-3910(95)00116-4.

[41] Vyazovkin SV, Lesnikovich AI. Error in determining activation energy caused by the wrong choice of process model. Thermochim Acta 1990;165:11–5. doi:10.1016/0040-6031(90)80201-9.

[42] Budrugeac P, Homentcovschi D, Segal E. Critical considerations on the isoconversional methods III. On the evaluation of the activation energy from non-isothermal data. J Therm Anal Calorim 2001;66:557–65. doi:10.1023/A:1013129304353.

[43] Vyazovkin S, Wight CA. Model-free and model-fitting approaches to kinetic analysis of isothermal and nonisothermal data. Thermochim Acta 1999;340–341:53–68. doi:10.1016/S0040-6031(99)00253-1.

[44] Scully K, Bissessur R. Decomposition kinetics of nylon-6/graphite and nylon-6/graphite oxide composites. Thermochim Acta 2009;490:32–6. doi:10.1016/j.tca.2009.01.029.

[45] Pashaei S, Siddaramaiah S, Avval M, Syed A. Thermal degradation kinetics of nylon6/GF/crysnano nanoclay nanocomposites by TGA. Chem Ind Chem Eng Q 2011;17:141–51. doi:10.2298/CICEQ101007064P.

[46] Zuo X, Shao H, Zhang D, Hao Z, Guo J. Effects of thermal-oxidative aging on the flammability and thermal-oxidative degradation kinetics of tris(tribromophenyl) cyanurate flame retardant PA6/LGF composites. Polym Degrad Stab

2013;98:2774–83. doi:10.1016/j.polymdegradstab.2013.10.014.

[47] ASTM E1641-15. West Conshohocken, U.S.: ASTM International; 2015. doi:10.1520/E1641.

[48] Aharoni SM. n-Nylons: their Synthesis, Structure and Properties. Chichester : John Wiley & Sons,; 1997.

[49] Aharoni SM. Crystallinity and Poymorphism in the n-Nylon Family. n-Nylons Their Synth. Struct. Prop., Chichester, UK: John Wiley & Sons Ltd; 1997, p. 34–70.

[50] Kyotani M, Mitsuhashi S. Studies on Crystalline Forms of Nylon 6. II Crystallization from the Melt. J Polym Sci 1972;10:1497–508.

[51] Liu X, Wu Q. Phase transition in nylon 6/clay nanocomposites on annealing. Polymer (Guildf) 2002;43:1933–6. doi:10.1016/S0032-3861(01)00759-5.

[52] Fornes TD, Paul DR. Crystallization behavior of nylon 6 nanocomposites. Polymer (Guildf) 2003;44:3945–61. doi:10.1016/S0032-3861(03)00344-6.

[53] Campoy I, Gomez MA, Marco C. Structure and thermal properties of blends of nylon 6 and a liquid crystal copolyester. Polymer (Guildf) 1998;39:6279–88. doi:10.1016/S0032-3861(98)00181-5.

[54] Hiramatsu N, Hirakawa S. Melting and Transformation Behavior of gamma form nylon6 under high pressure. Polymer (Guildf) 1982;14:165–71.

[55] Avramova N. Study of the healing process of polymers with different chemical structure and chain mobility. Polymer (Guildf) 1993;34:1904–7. doi:10.1016/0032-3861(93)90433-B.

Chapter 2

2 Thermal Properties of Glass Fiber Reinforced Polyamide 6 Composites Throughout the Direct Long-Fiber Reinforced Thermoplastic Process

2.1 Introduction

Recently, the direct long-fiber reinforced thermoplastic (D-LFT) process, in which continuous fiber rovings are fed directly into a polymer melt, has been gaining acceptance from the automotive industry [1]. The D-LFT process, depicted in Figure 2.1, creates a more streamlined process sequence than typical injection molding or compression molding processes. The removal of semi-finished products reduces process cost as well as eliminates additional heating and plastification to make finished products, thus decreasing the degradation of the material and the amount of process stabilizers required. This process also allows manufacturers to work with raw materials and make modifications for part optimization in the final products while maintaining long fiber lengths, which leads to better mechanical properties [1]. Polypropylene (PP) has been widely used as a polymer matrix in the D-LFT process because of its good processability, its ability to be tailored for specific applications, and its retention of mechanical properties after recycling [2]. However, it has relatively lower mechanical properties and service temperatures, which may limit its usage in several applications.

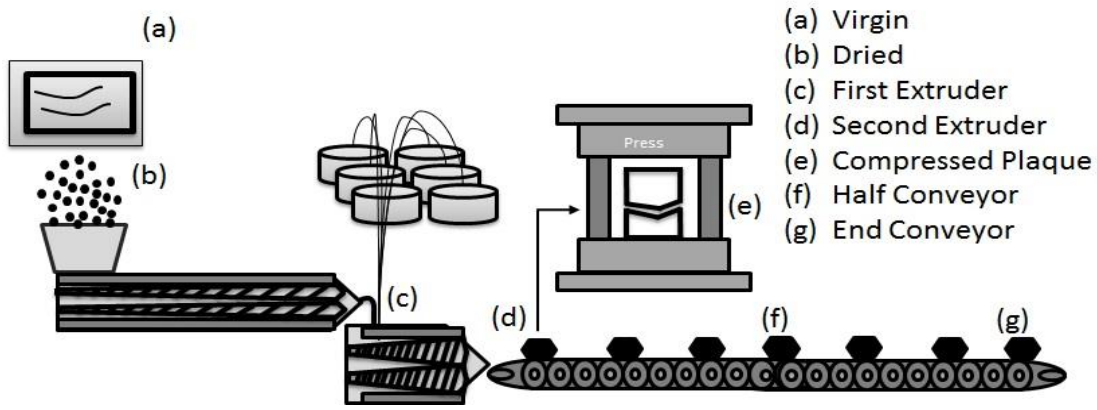

Figure 2.1 Schematic of D-LFT process with indicated locations for sample collection.

Polyamides are also candidates as polymer matrices used in the D-LFT process. Material characteristics of polyamides include high toughness over a large range of temperatures, good impact and abrasion resistance, lubricity, and resistance to organic solvents [3]. Polyamides as an engineering polymer have a range of possible applications, including those requiring thermal stability, fire resistance, and good mechanical properties [3] and, consequently, have been an area of great study [4][5]. Despite their attractive properties, polyamides' potential performance can be limited by their susceptibility to degradation during processing [3][6][7][8][9][10]. It was reported that properties of polyamide 6 (PA6) and/or glass fiber reinforced PA6 composites decreased after multiple injection molding process cycles [11][12][13][14] and multiple extrusion process cycles [15]. The results of these studies are significant to this current research because two extruders are used in the D-LFT process.

During the D-LFT process, which includes an oven to dry a material, two extruders, a conveyer and a press, there are three types of degradation mechanisms PA6 has the

potential to undergo: thermal [3][16], mechanical [14], and thermo-oxidative [3,17]. Awareness of these mechanisms and the effect they have on material properties are of high importance during polymer processing to ensure product consistency and process optimization. This study investigates viscosity number (VN), apparent activation energy for decomposition, and crystallization behavior of PA6 matrix in glass fiber reinforced PA6 as a function of location in the D-LFT process, and provides insight into how these properties of PA6 change during the D-LFT process.

2.2 D-LFT Process

Polymer and fibers go through various types of equipment in the D-LFT process. The following section reviews the D-LFT process stages and discusses their potential influences on polymer degradation.

2.2.1 Pre-Drying

PA6 and other polyamides are well known for their water absorption tendency [6][18]. Absorbed water can have negative effects, through hydrolysis, on polyamides' molecular structure and physical properties (such as tensile, flexural, and impact strength) and, therefore, must be removed prior to processing at elevated temperatures [6][18]. An improper pre-drying cycle can also affect the appearance of the finished product, through the appearance of silver streaks on the surface.

2.2.2 Compounding Twin Screw Extruder

The compounding co-rotating twin screw extruder, the first extruder used in the process, is dosed with dry polymer pellets via gravimetric feeding. The pellets are melted and thoroughly mixed as they are moved along this extruder. Within the extruder, high

temperatures and elevated mechanical shear stress can cause further degradation of the polyamides by decreasing the molecular weight of the polymer chains [15].

2.2.3 Waterfall Film Die

At the end of the compounding extruder, a film die transfers the molten plastic into the mixing extruder, the second extruder used in the process. The plastic is briefly introduced to atmospheric conditions at a molten state as it flows into the mixing extruder. This exposure can potentially cause thermo-oxidative degradation of polyamides [3].

2.2.4 Mixing Twin Screw Extruder

The mixing twin screw extruder receives molten plastic from the film die as well as continuous fiber rovings from bobbins and combines them. This extruder uses co-rotating twin screws to shear the continuous fibers and integrate them with the polymer melt, producing a mixture called the plastificate. This extrusion process exposes the composite melt to elevated temperatures and higher mechanical shear conditions which can cause additional degradation. Once fibers have been wetted by the polymer melt as well as dispersed and distributed in the polymer melt, the resulting plastificate is ejected from the mixing extruder's rectangular die onto the conveyor.

2.2.5 Conveyor

The conveyor serves two purposes in the D-LFT process: (i) to cut the extruded materials into appropriate shot sizes using a cutting shear, and (ii) to transfer the plasticifacte to the compression press. Heaters surrounding the conveyor maintain the temperature of the plastificate during the transit. The plastificate is exposed to atmospheric conditions along the conveyor. This atmospheric exposure, combined with the elevated

temperature of the conveyor, has the potential to cause further thermo-oxidative degradation.

2.2.6 Compression Molding

The final stage in the process is compression molding, wherein a press uses high pressure to shape the plastificate into the final part as well as a relatively cold mold to solidify the thermoplastic matrix. Flow of plastificate in the mold under the high pressure and rapid decrease in temperature have the potential to degrade the polymer matrix. In this study, plastificates were transferred to the press as soon as they were cut on the conveyer (Figure 2.1) to minimize the thermo-oxidative degradation on the conveyer.

2.3 Experimental

2.3.1 Materials Fabrication of Composites

Ultramid® 8202 HS, supplied by BASF, was used as PA6 matrix, and StarRov® 886 RXN (in the form of rovings), provided by Johns Manville, was used as glass fiber reinforcement. The PA6 was dried in a dryer (LUXOR S 120, Motan Colotronic) at a set temperature of 80°C for 16 hours prior to being processed. The PA6 was combined with 30 wt% of the glass fibers using an industry-scale Dieffenbacher D-LFT line at the Fraunhofer Project Centre for Composites Research in University of Western Ontario. The D-LFT line includes a dryer, two extruders, a conveyer, and a 2,500-ton hydraulic press (DCP-U 2500/2200, Dieffenbacher). The two extruders are a compounding twin screw extruder (ZSE-60HP-28D, Leistritz), named the first extruder, and a mixing twin screw extruder (ZSG-75 P-17D, Leistritz), named the second extruder, the screws of which have a diameter of 60 mm and 75 mm, respectively, and a length to diameter ratio of 28 and 17,

respectively. The technical specifications of the extruder configurations of the first extruder and second extruder can be found in the appendix of this thesis. Temperatures of both extruders were set to 280°C, and the screw speeds of the first extruder and second extruder were set to 80 rpm and 50 rpm, respectively. Conveyer belt temperature was set to 260°C. For the hydraulic press, mold temperature was set to 120°C, and force applied to plastificates was set to 5,000 kN for 30 s.

Material samples were collected from seven locations along the D-LFT line representing various stages of processing. Specifically, material was taken (a) before processing (i.e., virgin PA6), (b) after the drying process when still in pellet form, (c) after the PA6 had melted in the first extruder (taken directly from the waterfall film die), (d) after the second extruder (once the fibers had been introduced), (e) when it was in the form of a compressed plaque, (f) when it was half-way along the conveyor and, finally, (g) at the end of the conveyor. A schematic indicating the points of sample collection along the process can be seen in Figure 2.1. It is noted that plastificates which were cut on the conveyer were either transferred to the hydraulic press (Figure 2.1e) or continued on the conveyer (Figure 2.1f and g).

2.3.2 Viscosity Number Measurement

As previously discussed, polymer degradation through heat, shear, oxidation, or a combination of the three mechanisms has an effect on the molecular structure of the polymer primarily through a decrease in the molecular weight. VN measurements were performed to analyze trends in molecular weight of PA6, because although not strictly correlated, the viscosity number of a PA6 solution is dependent on the molecular weight

of the polymer. Measurements were performed according to ISO 307:2007, using 96% sulfuric acid (H_2SO_4) as a solvent. *VN* (in mL/g) was calculated by

$$VN = \left(\frac{\eta}{\eta_0} - 1\right) \times \frac{1}{c} \quad (1)$$

where η is the viscosity (in Pa·s) of the PA6-sulfuric acid solution, η_0 is the viscosity (in Pa·s) of the sulfuric acid, and c is the concentration of the PA6 in the solution (0.005 g/mL).

2.3.3 Thermogravimetric Analysis

Thermal decomposition behaviors of the materials were examined using thermogravimetric analyzer (TGA) (SDT Q600, TA Instruments). To avoid any external reactions with oxygen, nitrogen was used as a purge gas (with a flow rate of 100mL/min into the cell). Samples of 8.5 mg (±0.5 mg) were heated at a rate of 20°C/min from room temperature to 250°C and were held at 250°C for 5 minutes, to ensure an isothermal temperature in the cell prior to decomposition. After these 5 minutes, the temperature was further increased to 500°C using one of the following heating rates: 1, 2, 5, or 10°C/min.

2.3.4 Differential Scanning Calorimetry

Non-isothermal and isothermal crystallization behaviours of the materials were characterized using DSC (Q200, TA Instruments). Sapphire and indium calibration samples were used for temperature and heat-of-fusion calibration, respectively. Mass of samples used for the DSC measurements was 8.5 mg (±0.5 mg). Nitrogen atmosphere was used in both analyses (isothermal and non-isothermal) with a flow rate of 50 mL/min. For non-isothermal crystallization, a sample was first heated to 270ºC at 10ºC/min and held at that temperature for 5 min to erase the thermal history. Then, the sample was cooled to

20ºC at 10ºC/min and held at that temperature for 5 min. Lastly, the sample was reheated to 270ºC at 10 ºC/min.

For isothermal crystallization, a sample was first heated to 270ºC at 10ºC/min and held at that temperature for 5 min to erase the thermal history. Then, the sample was cooled to the isothermal temperature of 200ºC at 50ºC/min and held at that temperature for 30 min to ensure complete crystallization.

2.4 Results and Discussion

2.4.1 Discoloration

Figure 2.2 shows color change of samples taken at the different stages along the D-LFT process. A slight color change is evident after drying. This color change was possibly due to air exposure in the convection oven causing the first signs of thermo-oxidative degradation while the moisture was removed from the PA6. The sample became yellow after the first extruder and then brown after the second extruder possibly due to the high temperature and mechanical shear stress. The sample got slightly darker after the press, whereas the color change was more significant after the conveyer possibly due to thermo-oxidative degradation.

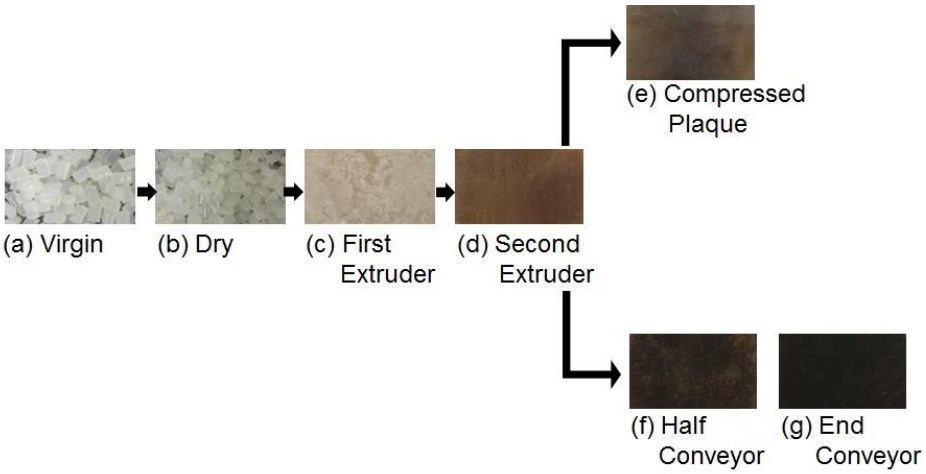

Figure 2.2 Material discoloration throughout D-LFT process.

2.4.2 Viscosity Number

Figure 2.3 shows the VNs corresponding to the different stages along the D-LFT process. Overall, VN decreased with process progression. The decrease in VN suggests that the molecular weight of the PA6 decreased during the manufacturing process, which is a result of the processing of the material imposed degradation on the PA6. However, it is interesting to note that VN (or molecular weight) decreased only slightly through the second extruder despite continuous glass fibers being fed into the second extruder.

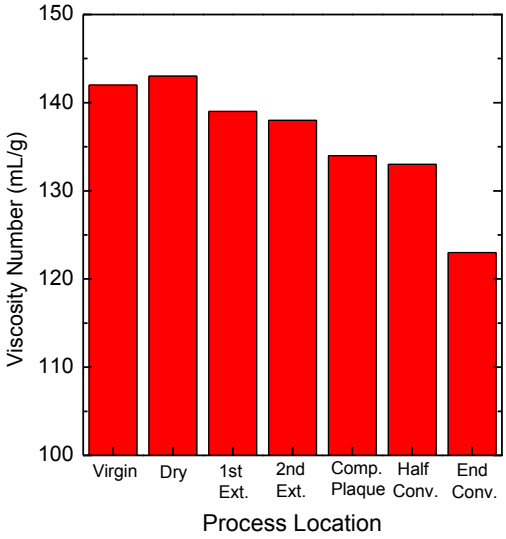

Figure 2.3 Viscosity number of materials collected along D-LFT process.

2.4.3 Thermal Decomposition

Figure 2.4 shows representative thermogravimetric curves for the heating rate of 2°C/min between 300°C and 500°C. These curves show a single-stage decomposition of the PA6. To quantify the matrix degradation level during the D-LFT process, kinetic changes in the decomposition profile were analyzed using the Ozawa/Flynn/Wall (O/F/W) method [19]. The experimentation and decomposition profile analysis done using this method follows ASTM E1641-15 [20].

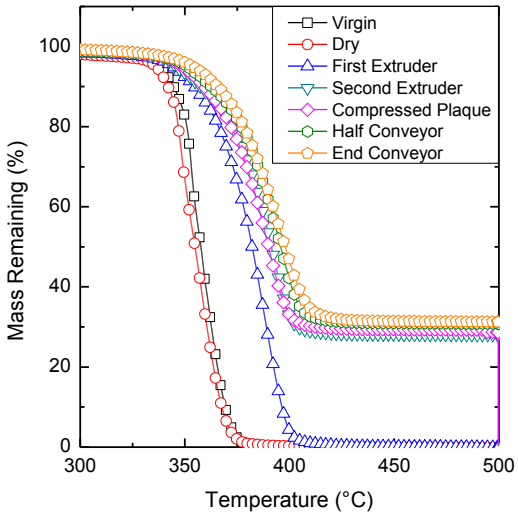

Figure 2.4 Typical TGA curves of materials collected from the D-LFT process at heating rate of 2 °C/min.

The degree of conversion, α, of the sample is calculated by

$$\alpha = \left(\frac{M_o - M_t}{M_o - M_f}\right) \times 100 \qquad (2)$$

where M_o, M_t, M_f are, respectively, the mass at the beginning of the decomposition profile, the corresponding mass at the decomposition level being calculated (e.g. mass when 20% decomposed), and the final mass after decomposition. In this study, α values of 5, 10, 15, 20, 40, and 60% were selected to investigate effects of α on activation energy for decomposition. The kinetic analysis of this decomposition profile assumes that the rate of conversion is linearly related to the temperature-dependent rate constant, *k(T)*, and temperature independent function to the conversion, i.e.

$$\frac{\mathrm{d}\alpha}{\mathrm{d}t} = k(T)f(\alpha) \tag{3}$$

where *f(α)* is dependent on the reaction degradation mechanism.

The Arrhenius equation is used to describe the function *k(T)*:

$$k(T) = A\, e^{-\frac{E}{\mathrm{RT}}} \tag{4}$$

where *T* is temperature (K), *A* is the pre-exponential factor, *E* is the activation energy, and *R* is the gas constant (8.31 J $mol^{-1}K^{-1}$).

Decomposition occurs under a constant heating rate, so $\beta = \mathrm{d}T/\mathrm{d}t$ can be substituted into *Eq. 3* thus:

$$\beta \frac{\mathrm{d}\alpha}{\mathrm{d}T} = Af(\alpha)e^{-\frac{E}{RT}} \tag{5}$$

Integrating over the variables α and T [21] gives

$$F(\alpha) = \int_0^{\alpha} \frac{\mathrm{d}\alpha}{f(\alpha)} = A\beta^{-1} \int_{T_0}^{T} e^{-\frac{E}{RT}}\, dT \tag{6}$$

If the initial temperature, T_0, is well below the temperatures of measurable reaction rates, the lower limit of the temperature integral can be ignored. Next, we define $x = -E/RT$ and obtain the following equation:

$$F(\alpha) = \left(\frac{AE}{\beta R}\right)\left\{-\frac{e^x}{x} + \int_{-\infty}^{x} \left(\frac{e^x}{x}\right) dx\right\} = \left(\frac{AE}{\beta R}\right) p(x) \tag{7}$$

Activation energy is calculated based on the assumption that decomposition obeys first-order kinetics, that is, p(x) is a linear function and can be solved using the Doyle approximation. In the following equation, E_a represents the apparent activation energy derived from the Doyle approximation.

$$E_a = -\left(\frac{R}{b}\right)\Delta \log[\beta] \,/\Delta\left(\frac{1}{T}\right) \tag{8}$$

In this equation, b is the logarithm of the approximation derivative.

Figure 2.5 shows Ozawa plots, i.e., how the logarithm of heating rate relates to the inverse of temperature for all α values. The figure indicates that the slopes of trend lines for all the α values were almost linear, and the slope decreased with the increase of α value at each given process location (from (a) the virgin samples to (g) the end conveyor samples). When slopes at different process locations are compared for a given α value, the slope increased with process progression. The slopes of trend lines were used to calculate E_a values.

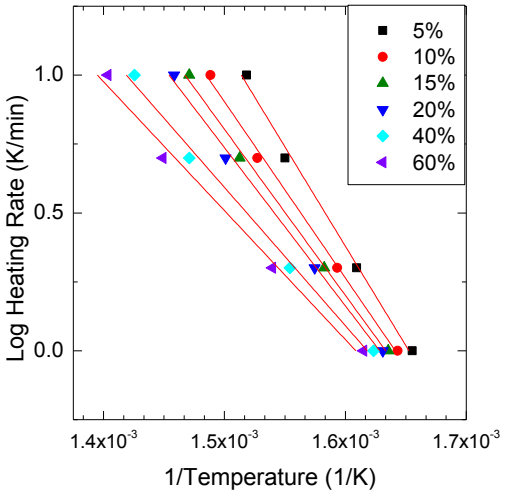
5%
10%
15%
20%
40%
60%
Log Heating Rate (K/min)
1.0
0.5
0.0
1.4x10-3
1.5x10-3
1.6x10-3
1.7x10-3
1/Temperature (1/K)

(a)

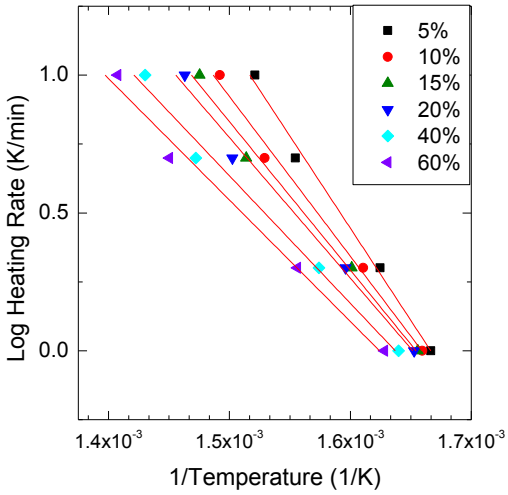
5%
10%
15%
20%
40%
60%
Log Heating Rate (K/min)
1.0
0.5
0.0
1.4x10-3
1.5x10-3
1.6x10-3
1.7x10-3
1/Temperature (1/K)

(b)

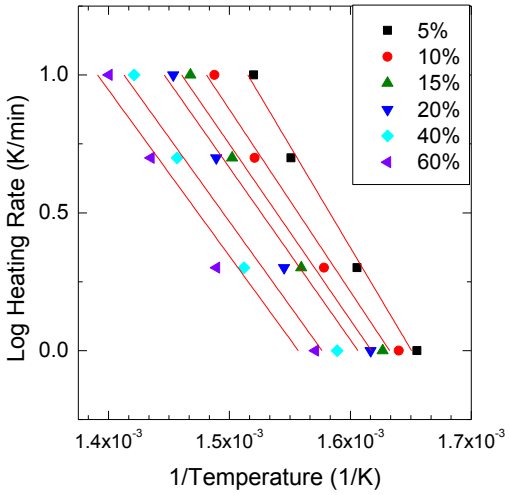
5%
10%
15%
20%
40%
60%
Log Heating Rate (K/min)
1.0
0.5
0.0
1.4x10-3
1.5x10-3
1.6x10-3
1.7x10-3
1/Temperature (1/K)

(c)

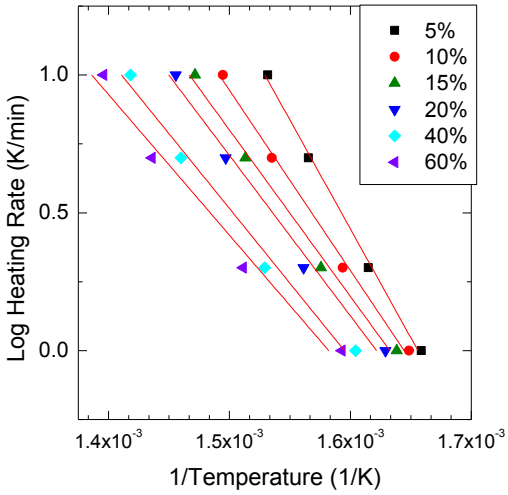
5%
10%
15%
20%
40%
60%
Log Heating Rate (K/min)
1.0
0.5
0.0
1.4x10-3
1.5x10-3
1.6x10-3
1.7x10-3
1/Temperature (1/K)

(d)

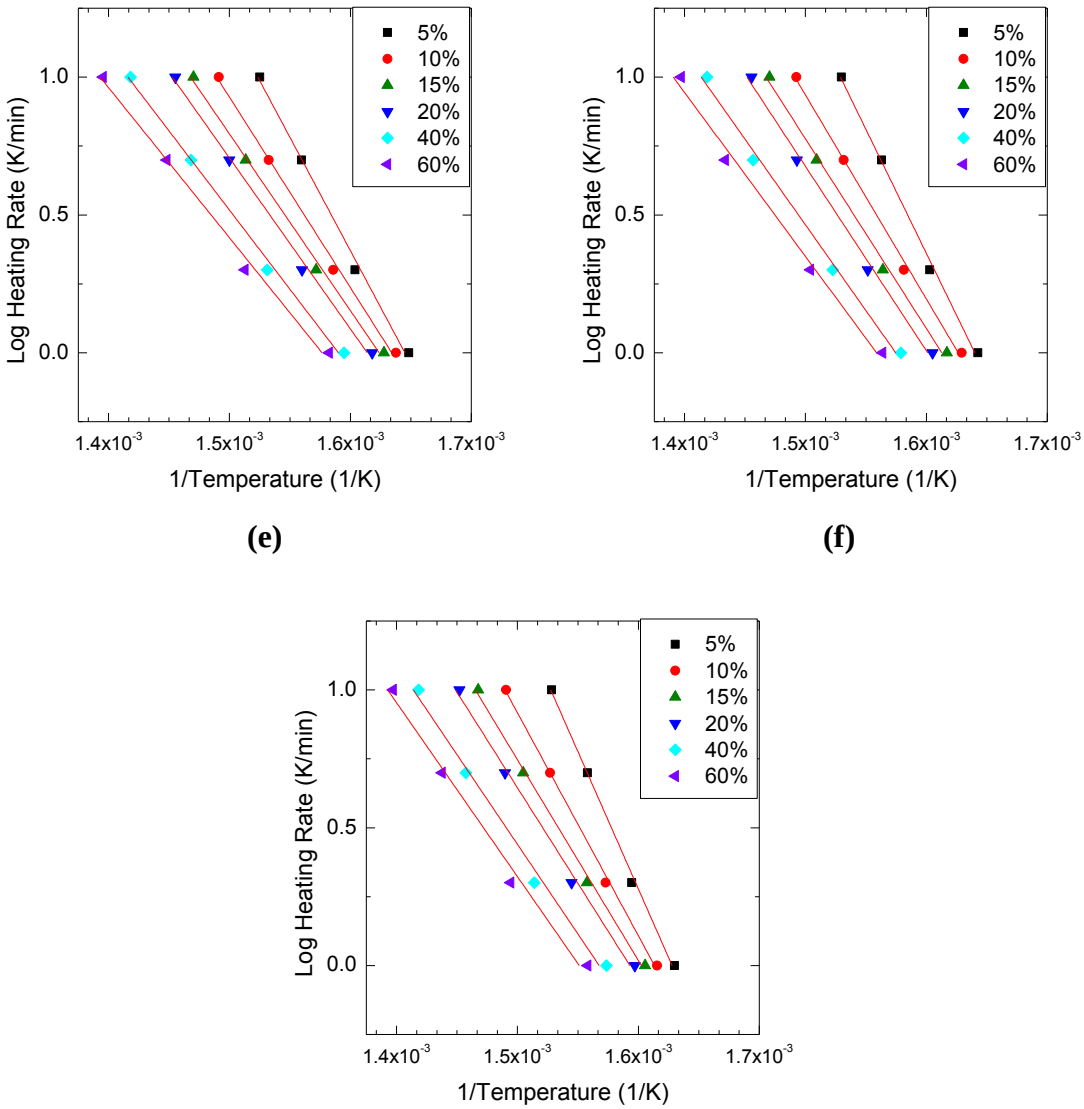

(e) **(f)**

(g)

Figure 2.5 Ozawa plots of materials collected from the D-LFT process at different conversions: (a) virgin samples, (b) dry samples, (c) first extruder samples, (d) second extruder samples, (e) compressed plaque samples, (f) half conveyor samples, and (g) end conveyor samples.

Figure 2.6 shows E_a as a function of α at all seven process locations (Figure 2.6a for the virgin, dry, and first extruder samples and Figure 2.6b for the second extruder, compressed plaque, half conveyor, and end conveyor samples). It can be seen that E_a

decreases with increasing α (i.e., increasing decomposition). Coversely, E_a values were greater in samples collected farther along the process: the virgin and dried samples < the first extruder and second extruder samples as well as compressed plaque samples < the half conveyor samples < the end conveyor samples. A possible explanation for this observation is that the content of char generated in the materials increases through the D-LFT process. It was previously postulated that the presence of char can influence activation energy [17][22]. Further research into the causing mechanisms of this increase is required.

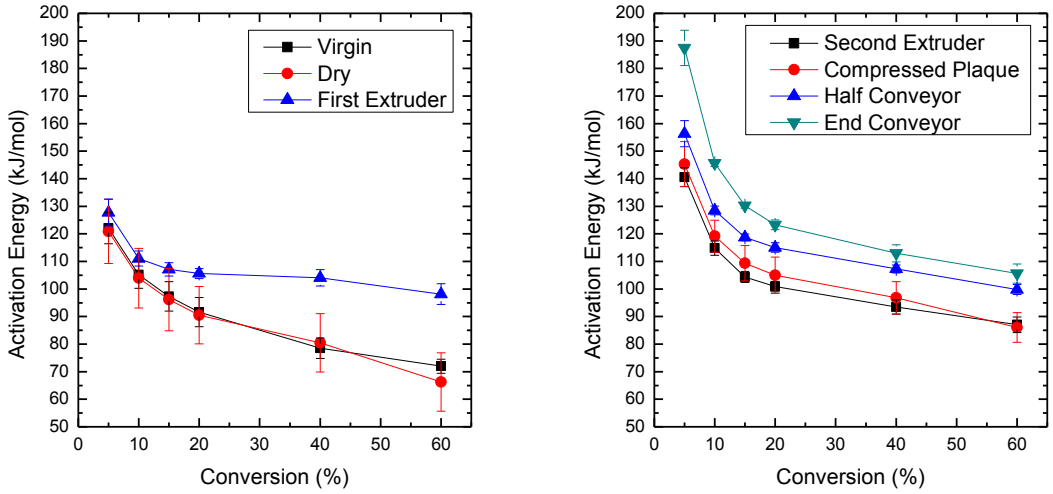

(a) **(b)**

Figure 2.6 Activation energy throughout decomposition of materials collected from the D-LFT process: (a) PA6 and (b) PA6 composites.

2.4.4 Crystallization

2.4.4.1 Non-Isothermal Crystallization

Figure 2.7 shows non-isothermal DSC cooling curves (Figure 2.7a) and subsequent heating curves (Figure 2.7b) of materials throughout the D-LFT process. The thermal properties obtained from the DSC cooling and heating curves are summarized in Table 2.1, which includes crystallization peak temperature (T_c), enthalpy of crystallization (ΔH_c), melting peak temperatures (T_{m1}, T_{m2}), enthalpy of fusion (ΔH_m) and degree of crystallinity (X_c). The degree of crystallinity $\boldsymbol{X_c}$ of the sample was calculated from the DSC heating curve and the following equation:

$$X_c = \frac{\Delta H_m}{\Delta H_f (1 - W_f)} \times 100\% \quad (9)$$

where ΔH_m is enthalpy of fusion; ΔH_f is enthalpy of fusion of fully crystalline PA6, which is taken to be 230 J/g [23]; and W_f is the weight fraction of fiber.

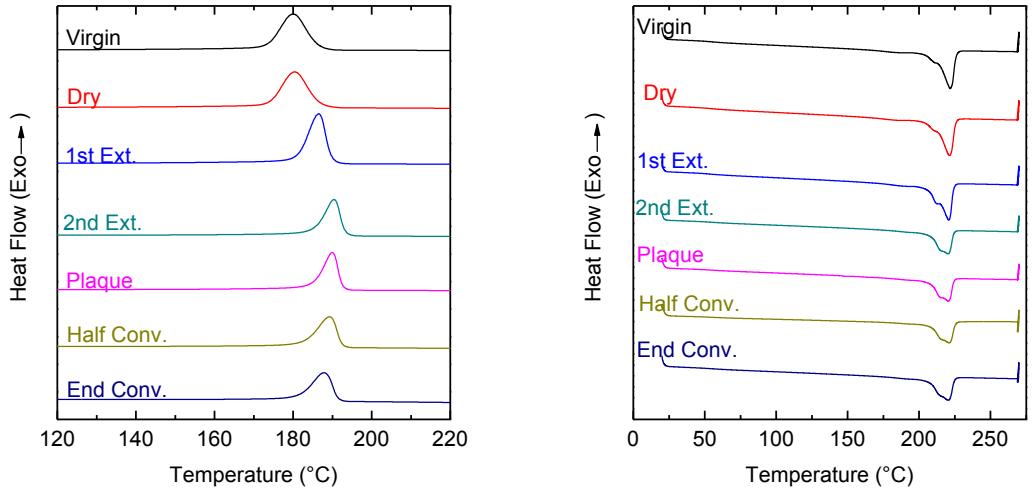

(a) (b)

Figure 2.7 Non-isothermal DSC curves of materials collected from the D-LFT process: (a) cooling curves and (b) heating curves.

DSC cooling curves (Figure 2.7a) illustrate that the virgin and dried samples had the lowest crystallization temperatures around 180°C. The first extruder samples had 186°C, and the samples collected later in the process had crystallization temperatures closer to 190°C. The two melting peaks (T_{m1} and T_{m2}, where $T_{m1} < T_{m2}$) on the DSC heating curves (Figure 2.7b) are associated with a difference in melting temperatures between the two phases present in the morphology (α and γ) [4,24,25]. The α-phase has polymer chains fully extended and oriented in an anti-parallel fashion while the γ-phase has polymer chains twisted at an angle of approximately 60° in order to maintain complete satisfaction of hydrogen bonds. With process progression, the first melting peak gradually became more pronounced which could be a result of the amount of γ-phase increasing, which has a different melting behavior from the α-phase [26]. Table 2.1

shows that T_{m1} was slightly increased by fiber addition, but T_{m2} remained constant. Table 2.1 also shows the calculated degree of crystallinity $\boldsymbol{X_c}$ for each of the process locations. Degree of crystallinity values were similar among the different process locations.

Table 2.1 Non-isothermal crystallization data of materials collected from the D-LFT process. The numbers in the parenthesis are the standard deviations (n=3).

Process Location	T_c (ºC)	ΔH_c (J/g)	T_{m1} (ºC)	T_{m2} (ºC)	ΔH_m (J/g)	X_c (%)
Virgin	180.3 (0.2)	62.5 (0.6)	211.1 (0.6)	221.9 (0.2)	65.7 (2.1)	28.6 (0.9)
Dried	180.3 (0.1)	61.1 (1.0)	210.6 (0.6)	221.9 (0.5)	66.9 (1.7)	29.1 (0.7)
First Extruder	186.4 (0.2)	60.7 (1.2)	212.4 (0.6)	221.0 (0.1)	68.3 (1.4)	29.7 (0.6)
Second Extruder	190.5 (0.1)	41.3 (0.7)	215.2 (0.6)	220.7 (0.2)	48.1 (1.6)	29.5 (1.0)
Compressed Plaque	190.2 (0.2)	41.2 (0.9)	215.3 (0.2)	220.6 (0.2)	48.7 (3.8)	30.5 (2.4)
Half Conveyor	189.6 (0.4)	40.8 (1.4)	216.0 (0.4)	221.4 (0.5)	45.4 (3.9)	27.9 (2.4)
End Conveyor	188.7 (0.6)	41.0 (0.6)	215.1 (0.6)	220.5 (0.4)	47.1 (1.5)	29.3 (0.9)

2.4.4.2 Isothermal Crystallization

Figure 2.8 shows isothermal DSC curves of materials throughout the D-LFT process. The figure suggests that crystallization speed was increased after the first extruder, and further increased after the second extruder. Using the isothermal DSC curves, relative degree of crystallinity X_{rel} was calculated as follows:

$$X_{rel} = \frac{\int_0^t \frac{dH(t)}{dt} dt}{\int_0^\infty \frac{dH(t)}{dt} dt} \tag{10}$$

where the isothermal DSC curve is integrated between t = 0 and t, and divided by the overall crystallization area.

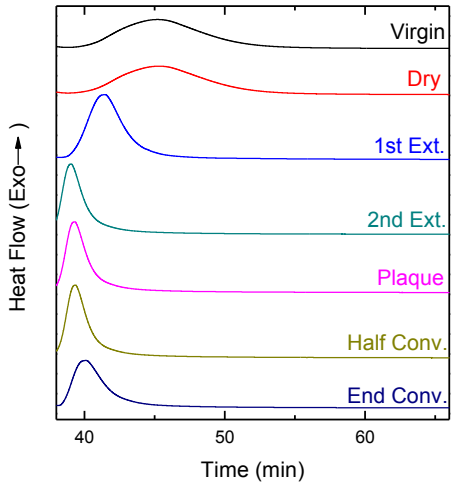

Figure 2.8 Isothermal DSC crystallization curves of materials collected from the D-LFT process.

The crystallization kinetics were analyzed using the Avrami equation. According to the Avrami model [27,28], the relative degree of crystallinity X_{rel} is described as follows:

$$X_{rel}(t) = 1 - \exp(-kt^n) \tag{11}$$

where n is the Avrami exponent that depends on the nucleation mechanism and growth geometry of crystals, k is the crystallization rate constant that involves both nucleation and growth rate parameters, and t is time.

Eq. 11 can be transformed into the double-logarithmic form,

$$\log[-\ln(1 - X_{rel}(t))] = \log k + n \log t \tag{12}$$

The parameters n (slope) and k (intercept) were determined by plotting $\log[-\ln(1 - X_{rel}(t))]$ against $\log t$. The crystallization half time $t_{1/2}$, which is defined as the time from crystallization onset until 50% completion, was calculated as follows:

$$t_{1/2} = \left(\frac{\ln 2}{k}\right)^{\frac{1}{n}} \tag{13}$$

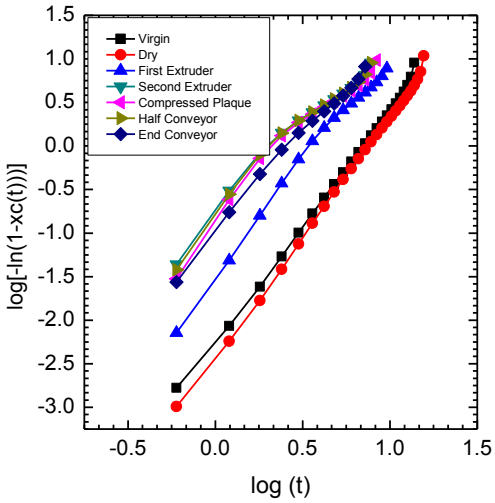

Figure 2.9 Avrami plots of materials collected from the D-LFT process.

Figure 2.9 shows Avrami plots, that is, plots of $\log[-\ln(1 - X(T))]$ versus $\log t$, of sample locations, where almost linear results were obtained from all the samples. Three distinct groups were observed: (1) the virgin and dried samples, (2) the first extruder samples, and (3) the second extruder, compressed plaque, half conveyer, and end conveyer

samples. In addition, a left shift of the lines occurred with progression in the process. Kinetic parameters determined by the Avrami equation are summarized in Table 2.2.

Table 2.2 Avrami parameters of materials collected from the D-LFT process. The numbers in the parenthesis are the standard deviations (n=3).

Sample	*n*	*k* (min^{-n})
Virgin	2.69 (0.03)	$5.24x10^{-3}$ ($2.27x10^{-4}$)
Dried	2.74 (0.04)	$4.02x10^{-3}$ ($3.08x10^{-4}$)
First Extruder	2.63 (0.15)	$2.87x10^{-2}$ ($6.25x10^{-3}$)
Second Extruder	1.88 (0.08)	$1.95x10^{-1}$ ($3.07x10^{-3}$)
Compressed Plaque	2.19 (0.12)	$1.23x10^{-1}$ ($4.94x10^{-2}$)
Half Conveyor	1.99 (0.12)	$1.74x10^{-1}$ ($1.90x10^{-2}$)
End Conveyor	2.19 (0.29)	$1.04x10^{-1}$ ($3.15x10^{-2}$)

The Avrami constant n decreased with glass fiber addition, which suggests that glass fiber addition had an influence on crystal nucleation mechanisms in PA6.

Figure 2.10 shows crystallization half-time from samples collected at each process location. The two most substantial decreases in crystallization half-time occurred in the material collected after the first and second extruders. The first decrease, which occurred after the first extruder, was possibly due to the decrease occurring in the molecular weight [15]. Polymer materials with lower molecular weight have a greater possible chain mobility and allow for crystallization to occur more rapidly [14]. Fornes and Paul [29] reported that extruded material showed faster crystallization than virgin material, and discussed reasons for this finding; namely, (1) decreased molecular weight, (2) impurities incorporated during extrusion creating nucleation sites, and/or (3) memory effects imposed upon the polymer

during extrusion and remaining during thermal analysis. The latter two factors may also have contributed to the decreases in crystallization half-time observed in this study.

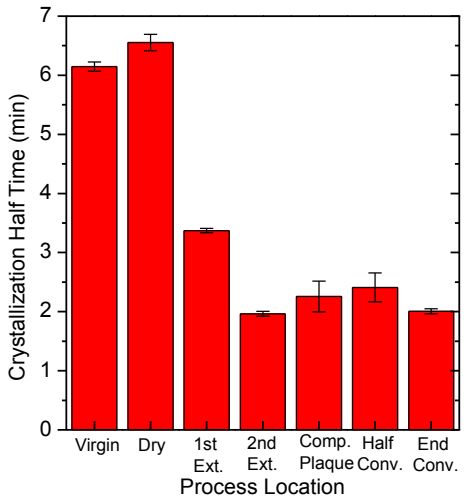

Figure 2.10 Crystallization half-time of materials collected from the D-LFT process.

The second decrease, which occurred after the second extruder, was possibly a result of the slight decrease occurring in the molecular weight and/or the incorporation of glass fibers at this stage of the process. Fibers when introduced to a polymer can act as heterogeneous nucleating agents (NA) during crystallization [24,30,31]. If the fibers do act in such a way, they may have provided nucleation sites for crystal growth and decreased the time required for crystallization. Further research is required to determine the precise mechanisms responsible for the decreased crystallization half-time.

2.5 Conclusions

Effects of the D-LFT process on the molecular weight and thermal properties of glass fiber reinforced PA6 were studied at seven locations. Results from the VN measurement showed that VN and, by extension, molecular weight decreased as the D-LFT process continued. TGA results showed that apparent activation energy of all samples decreased with increasing conversion values, whereas apparent activation energy increased with each process stage. Non-isothermal DSC crystallization analysis revealed no substantial changes to the material's degree of crystallinity during the process; however, isothermal DSC crystallization analysis showed a decrease in crystallization half-time occurring primarily after the first extruder and again after fiber incorporation (i.e., after the second extruder).

References

[1] Schemme M. LFT – development status and perspectives. Reinf Plast 2008;52:32–9. doi:10.1016/S0034-3617(08)70036-5.

[2] Balow MJ. Growth of Polypropylene Usage as a Cost-Effective Replacement of Engineering Polymers. In: Karian HG, editor. Handb. Polypropyl. Polypropyl. Compos., Basel, New York: Marcel Dekker, Inc.; 1999, p. 1–15.

[3] Levchik SV, Weil ED, Lewin M. Thermal decomposition of aliphatic nylons. Polym Int 1999;48:532–57. doi:10.1002/(sici)1097-0126(199907)48:7<532::aid-pi214>3.0.co;2-r.

[4] Aharoni SM. n-Nylons: their Synthesis, Structure and Properties. Chichester : John Wiley & Sons,; 1997.

[5] Kohan MI. Nylon Plastics. New York, Wiley; 1973.

[6] Pedroso AG, Mei LHI, Agnelli JAM, Rosa DS. The influence of the drying process time on the final properties of recycled glass fiber reinforced polyamide 6. Polym Test 2002;21:229–32. doi:10.1016/S0142-9418(01)00074-5.

[7] Davis RD, Gilman JW, VanderHart DL. Processing degradation of polyamide 6/montmorillonite clay nanocomposites and clay organic modifier. Polym Degrad Stab 2003;79:111–21. doi:10.1016/S0141-3910(02)00263-X.

[8] Kohan MI. Nylon Plastics Handbook. New York: Hanser Publishers; 1995.

[9] Pielichowski K, Njuguna J. Thermal Degradation of Polymeric Materials. Rapra Technology Limited; 2005.

[10] Lehrle RS, Parsons IW, Rollinson M. Thermal degradation mechanisms of Nylon 6 deduced from kinetic studies by pyrolysis-g.c. Polym Degrad Stab 2000;67:21–33. doi:10.1016/S0141-3910(99)00112-3.

[11] Pedroso A., Mei LH., Agnelli JA., Rosa D. Properties that characterize the propagation of cracks of recycled glass fiber reinforced polyamide 6. Polym Test 1999;18:211–5. doi:10.1016/S0142-9418(98)00020-8.

[12] Lozano-González MJ, Rodriguez-Hernandez MT, Gonzalez-De Los Santos EA, Villalpando-Olmos J. Physical–mechanical properties and morphological study on nylon-6 recycling by injection molding. J Appl Polym Sci 2000;76:851–8. doi:10.1002/(SICI)1097-4628(20000509)76:6<851::AID-APP11>3.0.CO;2-D.

[13] Su K-H, Lin J-H, Lin C-C. Influence of reprocessing on the mechanical properties and structure of polyamide 6. J Mater Process Technol 2007;192–193:532–8. doi:10.1016/j.jmatprotec.2007.04.056.

[14] Crespo JE, Parres F, Peydró MA, Navarro R. Study of rheological, thermal, and mechanical behavior of reprocessed polyamide 6. Polym Eng Sci 2013;53:679–88. doi:10.1002/pen.23307.

[15] Lee KH, Lim SJ, Kim WN. Rheological and thermal properties of polyamide 6 and polyamide 6/glass fiber composite with repeated extrusion. Macromol Res 2014;22:624–31. doi:10.1007/s13233-014-2086-x.

[16] Beyler CL, Hirschler MM. Thermal Decomposition of Polymers. SFPE Handb. Fire Prot. Eng. 4th ed., Quincy, U.S.: National Fire Protection Association; 2008, p. 110–31.

[17] Zuo X, Shao H, Zhang D, Hao Z, Guo J. Effects of thermal-oxidative aging on the flammability and thermal-oxidative degradation kinetics of tris(tribromophenyl) cyanurate flame retardant PA6/LGF composites. Polym Degrad Stab 2013;98:2774–83. doi:10.1016/j.polymdegradstab.2013.10.014.

[18] Bernstein R, Derzon DK, Gillen KT. Nylon 6.6 accelerated aging studies: Thermal-oxidative degradation and its interaction with hydrolysis. Polym Degrad Stab 2005;88:480–8. doi:10.1016/j.polymdegradstab.2004.11.020.

[19] Sengupta R, Sabharwal S, Bhowmick AK, Chaki TK. Thermogravimetric studies on Polyamide-6,6 modified by electron beam irradiation and by nanofillers. Polym Degrad Stab 2006;91:1311–8. doi:10.1016/j.polymdegradstab.2005.08.012.

[20] ASTM E1641-15. West Conshohocken, U.S.: ASTM International; 2015. doi:10.1520/E1641.

[21] Flynn JH. The Isoconversional Method for Determination of Energy of Activation at Constant Heating Rates Corrections for the Doyle approximation. J Therm Anal 1983;27:95–102. doi:10.1007/BF01907325.

[22] Scully K, Bissessur R. Decomposition kinetics of nylon-6/graphite and nylon-6/graphite oxide composites. Thermochim Acta 2009;490:32–6. doi:10.1016/j.tca.2009.01.029.

[23] Wunderlich B. Crystal Melting. Macromol. Phys., New York: Academic Press; 1973.

[24] Şanli S, Durmus A, Ercan N. Effect of nucleating agent on the nonisothermal crystallization kinetics of glass fiber- and mineral-filled polyamide-6 composites. J Appl Polym Sci 2012;125:E268–81. doi:10.1002/app.36231.

[25] Hiramatsu N, Hirakawa S. Melting and Transformation Behavior of gamma form nylon6 under high pressure. Polymer (Guildf) 1982;14:165–71.

[26] Aharoni SM. Crystallinity and Poymorphism in the n-Nylon Family. n-Nylons Their Synth. Struct. Prop., Chichester, UK: John Wiley & Sons Ltd; 1997, p. 34–70.

[27] Avrami M. Kinetics of phase change. II Transformation-time relations for random distribution of nuclei. J Chem Phys 1940;8:212–24.

[28] Avrami M. Granulation, phase change, and microstructure kinetics of phase change. III. J Chem Phys 1941;9:177–84.

[29] Fornes TD, Paul DR. Crystallization behavior of nylon 6 nanocomposites. Polymer (Guildf) 2003;44:3945–61. doi:10.1016/S0032-3861(03)00344-6.

[30] Liang J, Xu Y, Wei Z, Song P, Chen G, Zhang W. Mechanical properties, crystallization and melting behaviors of carbon fiber-reinforced PA6 composites. J Therm Anal Calorim 2014;115:209–18. doi:10.1007/s10973-013-3184-2.

[31] Göschel U, Lutz W, Davidson NC. The influence of a polymeric nucleating additive on the crystallisation in glass fibre reinforced polyamide 6 composites. Compos Sci Technol 2007;67:2606–15. doi:10.1016/j.compscitech.2006.12.005.

Chapter 3

3 Effects of Processing Parameters on Thermal Properties of Glass Fiber Reinforced Polyamide 6 Composites Throughout the Direct Long-Fiber Reinforced Thermoplastic Process

3.1 Introduction

The recent drive behind light weighting in the automotive industry is a result of the ever-increasing fuel efficiency regulations which have caused part suppliers to rethink processing techniques in order to leverage their capabilities for greater weight savings. One material processing technique that has received much attention, due to the potential for manufacturing high strength-to-weight ratio products quickly and efficiently, is the direct long-fiber reinforced thermoplastic (D-LFT) process [1]. The D-LFT process offers (i) removal of semi-finished products, which gives efficient and flexible manufacturing and (ii) final products with a high strength-to-weight ratio by maintaining long fiber lengths during processing [2].

The D-LFT process, depicted in Figure 3.1, is a one-stop manufacturing process starting from raw materials to a final product, and includes various types of equipment. The process is summarized as follows: dried polymer pellets are fed into the first twin-screw extruder to melt them. A film die, which is attached to the end of the first extruder, transfers the molten plastic into the second extruder. The plastic is briefly introduced to atmospheric conditions at a molten state as it flows from the film die into the second extruder. The molten plastic is then combined with continuous fibers in the second extruder to form what is called the plastificate. The plastificate is ejected from the second extruder

onto a conveyor where it is cut into an appropriate shot size using a shear cutter. Finally, the plastificate is transferred to a compression molding machine to shape and solidify the plastificate into the final part.

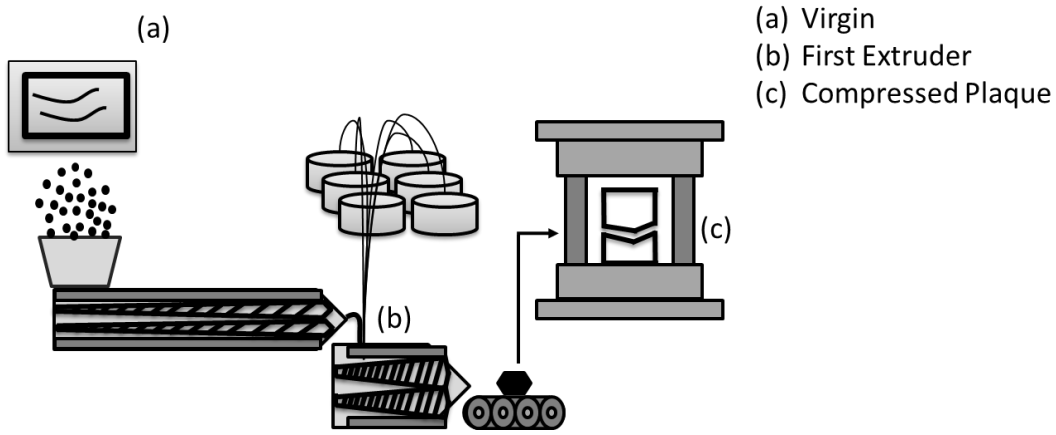

Figure 3.1 Schematic of D-LFT process with indicated locations for sample collection.

Polyamide 6 (PA6) is a good candidate as polymer matrix in the D-LFT process because it has high toughness over a large range of temperatures, good impact and abrasion resistance, lubricity, and resistance to organic solvents [3]. Despite its wide range of excellent properties, PA6 is susceptible to degradation [3][4][5][6][7][8]. When PA6 is used in the D-LFT process, PA6 has the potential to undergo thermal [3][9], mechanical [10], and thermo-oxidative [3], [11] degradation, and the molecular weight of PA6 is decreased [12]. As mentioned above, the D-LFT process includes tandem twin-screw extruders (i.e., the first and second extruders), which are the main components of the D-LFT process. The control of these extruders dictates productivity and properties of products. Therefore, it is important to understand how process parameters of the tandem twin-screw extruders in the D-LFT process influence material properties of PA6-based

composite materials. In this study, glass fiber reinforced PA6 composites were produced through the D-LFT process by changing barrel temperatures and screw speeds of the first and second twin-screw extruders. Viscosity number, apparent activation energy for decomposition, and crystallization behavior of the materials were characterized as a function of locations in the D-LFT process line.

3.2 Experimental

3.2.1 Materials and fabrication of composites

PA6 (Ultramid® 8202 HS, supplied in the form of pellets, BASF) was used as the matrix. The glass fiber (StarRov® 886 RXN, provided in the form of rovings, Johns Manville) was used as the reinforcement. The PA6 was first dried in a dryer (LUXOR S 120, Motan Colotronic) at a set temperature of 80°C for 16 hours. The PA6 was combined with 30 wt % of the glass fibers using an industry-scale Dieffenbacher D-LFT line at the Fraunhofer Project Centre for Composites Research at the University of Western Ontario. The D-LFT line includes a dryer, two extruders, a conveyer, and a 2,500-ton hydraulic press (DCP-U 2500/2200, Dieffenbacher). The two extruders are a compounding twin screw extruder (ZSE-60HP-28D, Leistritz), named the first extruder, and a mixing twin screw extruder (ZSG-75 P-17D, Leistritz), named the second extruder, the screws of which have a diameter of 60 mm and 75 mm, respectively, and a length to diameter ratio of 28 and 17, respectively. The length of the conveyor to the point where the plastificate was cut was approximately 50 cm, and conveyer belt temperature was set to 260°C. The cut plastificate was transferred to the press, and the transit time was about 5 s. For the hydraulic

press, mold temperature was set to 120°C, and force applied to the plastificate was set to 5,000 kN for 30 s.

Table 3.1 Process conditions of the first and second extruders used in the D-LFT process

Process Condition	Barrel Temperature (°C)	Screw Speed of 1st Extruder (rpm)	Screw Speed of 2nd Extruder (rpm)	Flow Rate from 2nd Extruder (kg/h)	Conveyor Speed (cm/s)
Standard Condition	280	80	50	102	1.2
Low Temperature	270	80	50	102	1.2
High Temperature	260	80	50	102	1.2
Low Screw Speed	280	40	25	51	0.6
High Screw Speed	280	161	100	205	2.3

The barrel temperature and screw speed of the two extruders were varied in this study, as summarized in Table 3.1. In the standard condition experiment, the temperature of both extruders was 280°C, and the screw speeds of the first and second extruders were 80 rpm and 50 rpm, respectively. To study effects of barrel temperature, the barrel temperatures of both extruders was changed to 270°C or 290°C. To examine effects of screw speed, the screw speeds of the first and second extruders were decreased, respectively, to 40 rpm and 25 rpm, or the screw speeds were increased, respectively, to 161 rpm and 100 rpm. Since the volume of material filled in the extruders was kept constant, the change of the screw speeds accompanied the change in flow rate of material from the second extruder: 102 kg/h for the standard condition, 51 kg/h for the low screw

speed setting and 205 kg/h for the high screw speed setting. Therefore, the conveyor speeds were changed as follows: 1.2 cm/s for the standard condition, 0.6 cm/s for the low screw speed setting, and 2.3 cm/s for the high screw speed setting. Table 3.2 shows approximate residence time of the D-LFT process for each process condition. The total process times with the low and high screw speeds are, respectively, around 1.8 times and 0.6 times as long as those with the standard, low temperature and high temperature conditions.

Table 3.2 Approximate residence time of the D-LFT process.

Process Condition	1st Extruder (s)	2nd Extruder (s)	Conveyor (s)	Transit (s)	Press (s)	Total Residence Time (s)
Standard Condition	66	43	42	5	30	186
Low Temperature	66	43	42	5	30	186
High Temperature	66	43	42	5	30	186
Low Screw Speed	131	86	83	5	30	335
High Screw Speed	33	21	22	5	30	111

Samples were collected from three locations along the D-LFT process line: (a) as received (i.e., virgin PA6), (b) directly after the first extruder (taken from the waterfall film die), and (c) a compressed plaque. A schematic indicating the points of sample collection along the process can be seen in Figure 3.1.

3.2.2 Viscosity number measurement

Viscosity number of a PA6 solution is dependent on the molecular weight of the PA6 though it is not strictly correlated. Viscosity number measurements were conducted

to give insight into changes in molecular weight during the process and under each process condition. Measurements were performed according to ISO 307:2007, using 96% sulfuric acid (H_2SO_4) as a solvent. Viscosity number *VN* (in mL/g) was calculated by

$$VN = \left(\frac{\eta}{\eta_0} - 1\right) \times \frac{1}{c} \tag{14}$$

where η is the viscosity (in Pa·s) of the PA6-sulfuric acid solution, η_0 is the viscosity (in Pa·s) of the sulfuric acid, and c is the concentration of the PA6 in the solution (0.005 g/mL).

3.2.3 Thermogravimetric analysis

Decomposition kinetics of both the polymer and composite samples were investigated using a thermogravimetric analyzer (TGA) (SDT Q600, TA Instruments). Mass of samples was 8.5 mg (±0.5 mg). The temperature profile of the TGA analysis conducted was as follows: (1) heating ramp of 20°C/min from room temperature to 250°C, (2) isothermal for 5 min to ensure homogeneous temperature distribution in the cell, and (3) temperature ramp from 250°C to 500°C using one of the following heating rates: 1, 2, 5, or 10°C/min. Nitrogen was used as a purge gas at a flow rate of 100 mL/min.

The decomposition kinetics of the PA matrix were analyzed using the Ozawa/Flynn/Wall (O/F/W) method [13]. The experimentation and calculation follow ASTM E1641-15 [14]. The degree of conversion, α, of the sample was calculated by

$$\alpha = \left(\frac{M_o - M_t}{M_o - M_f}\right) \times 100 \tag{15}$$

where M_o, M_t, M_f are, respectively, the mass at the beginning of the decomposition profile, the corresponding mass at the decomposition level being calculated (e.g. mass when 20% decomposed), and the final mass after decomposition. In this study, α values of 5, 10, 15, 20, 40, and 60% were selected to investigate effects of α on apparent activation energy for decomposition. Apparent activation energy E_a was calculated by

$$E_a = -\left(\frac{R}{b}\right)\Delta \log[\beta] \,/\Delta\left(\frac{1}{T}\right) \tag{16}$$

where R is the gas constant (8.31 J $mol^{-1}K^{-1}$), b is the logarithm of the approximation derivative, β is the heating rate (K/min), and T is temperature (K).

3.2.4 Differential scanning calorimetry

Non-isothermal and isothermal crystallization behaviours of the materials were studied using a differential scanning calorimeter (DSC) (Q200, TA Instruments). Temperature and heat-of-fusion were calibrated using sapphire and indium, respectively. A nitrogen purge gas with a flow rate of 50 mL/min was used. Mass of samples was 8.5 mg (±0.5 mg) in both non-isothermal and isothermal measurements. In non-isothermal crystallization measurements, a sample was first heated to 270ºC at 10ºC/min and held at that temperature for 5 min to erase the thermal history in the collected sample. The sample was then cooled to 20ºC at 10ºC/min and held at that temperature for 5 min. Lastly, the sample was reheated to 270ºC at 10ºC/min. The degree of crystallinity X_c of the sample was calculated from the second DSC heating curve and the following equation:

$$X_c = \frac{\Delta H_m}{\Delta H_f(1 - W_f)} \times 100\% \tag{17}$$

where ΔH_m is enthalpy of fusion; ΔH_f is enthalpy of fusion of fully crystalline PA6, which is taken to be 230 J/g [15]; and W_f is the weight fraction of fiber.

In the isothermal crystallization measurements, a sample was first heated to 270ºC at 10ºC/min and held at that temperature for 5 min to erase the thermal history of the collected sample. Then, the sample was cooled to the isothermal temperature of 200ºC at 50ºC/min and held at that temperature for 30 min to allow the sample to fully crystallize. Using the isothermal DSC curve, the relative degree of crystallinity X_{rel} was calculated as follows:

$$X_{rel} = \frac{\int_0^t \frac{dH(t)}{dt} dt}{\int_0^\infty \frac{dH(t)}{dt} dt} \tag{18}$$

where the isothermal DSC curve is integrated between $t = 0$ and t, and divided by the overall crystallization area.

The crystallization kinetics were analyzed using the Avrami equation. According to the Avrami model [16], [17], the relative degree of crystallinity X_{rel} is described as follows:

$$X_{rel}(t) = 1 - \exp(-kt^n) \tag{19}$$

where n is the Avrami exponent that depends on the nucleation mechanism and growth geometry of crystals, k is the crystallization rate constant that involves both nucleation and growth rate parameters, and t is time.

Eq. 19 can be transformed into the double-logarithmic form,

$$\log[-\ln(1 - X_{rel}(t))] = \log k + n \log t \tag{20}$$

The parameters n (slope) and k (intercept) were determined by plotting $\log[-\ln(1 - X_{rel}(t))]$ against $\log t$. The crystallization half time $t_{1/2}$, which is defined as the time from crystallization onset until 50% completion, was calculated as follows:

$$t_{1/2} = \left(\frac{\ln 2}{k}\right)^{\frac{1}{n}} \tag{21}$$

3.3 Results and discussion

3.3.1 Discoloration

Figure 3.2 shows color changes in the material throughout the D-LFT process under the different process conditions. Color of the virgin material changed yellow after the first extruder and then brown after the press in each process condition. The progressive discoloration of the material is possibly caused by accumulation of thermal, mechanical, and thermo-oxidative degradations. The compressed plaque samples processed with the low screw speed had the highest degree of discoloration, which could be a result of the longest process time, as shown in Table 3.2.

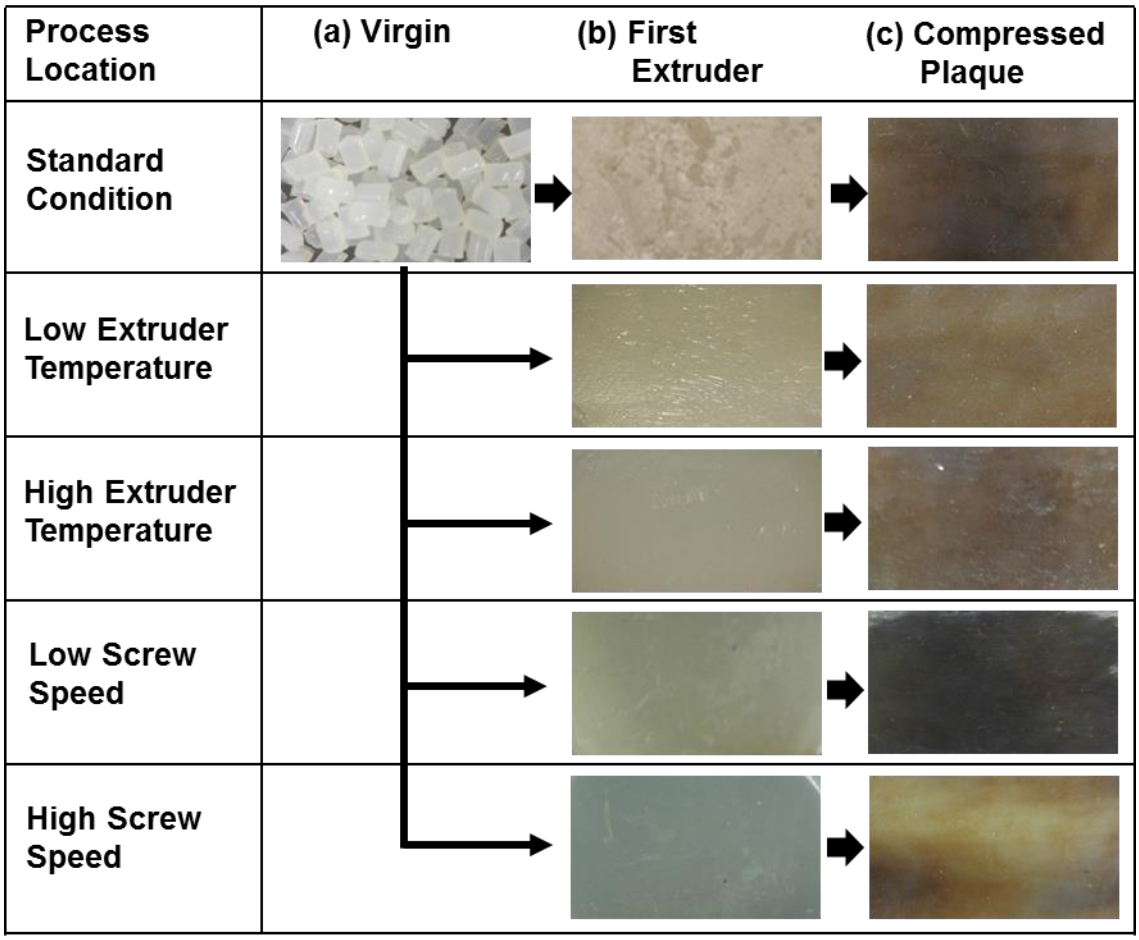

Figure 3.2 Material discoloration throughout D-LFT process with different process conditions.

3.3.2 Viscosity number

Figure 3.3 shows viscosity numbers of samples processed under different extruder temperatures (Figure 3.3a) and different screw speeds (Figure 3.3b). In each process condition, the viscosity number (or molecular weight) decreased with process progression from the first extruder to the compressed plaque, which is a result of thermal, mechanical, and thermo-oxidative degradations of the PA6 matrix.

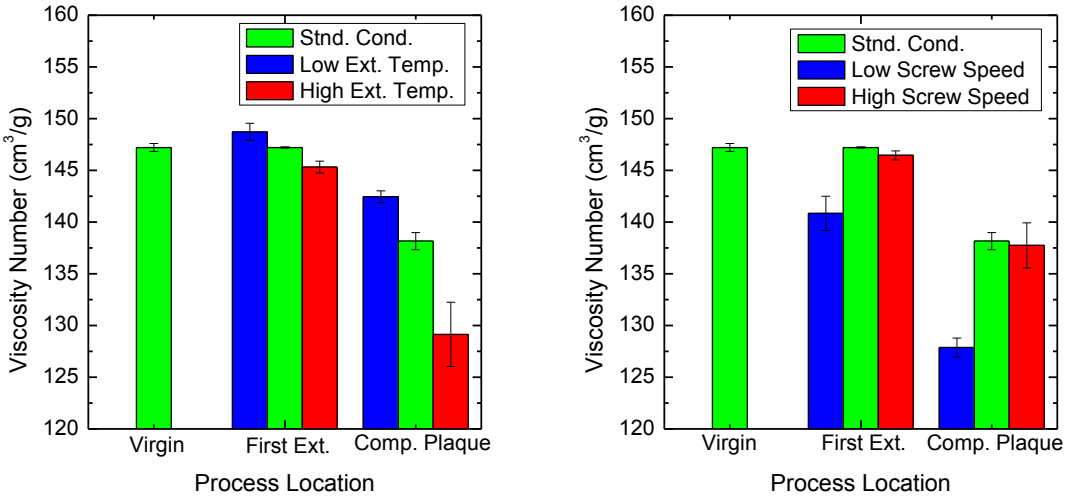

(a) (b)

Figure 3.3 Viscosity number of first extruder and compressed plaque samples processed under different (a) extruder temperatures and (b) screw speeds.

When samples processed at different extruder temperatures are compared (Figure 3.3a), the viscosity number (or molecular weight) decreased with increasing extruder temperature. The increase of extruder temperature may have promoted thermal and/or thermo-oxidative degradation of the PA6 matrix. When samples processed at different screw speeds are compared (Figure 3.3b), the viscosity number (or molecular weight) decreased with decreasing screw speed. Although the decrease of screw speed may have reduced mechanical degradation, the longer total process time could have promoted thermo-oxidative degradation which may have been the more predominant degradation mechanism that influences the viscosity number (or molecular weight).

3.3.3 Thermal decomposition

Figure 3.4 shows typical thermogravimetric profiles of first extruder samples (Figure 3.4a) and compressed plaque samples (Figure 3.4b) at a heating rate of 10°C/min

between 300°C and 500°C. The profiles were obtained from samples produced under different process conditions, and all the samples showed a single-stage decomposition of PA6. Figure 3.5 shows Ozawa plots, i.e., how the logarithm of heating rate relates to the inverse of temperature for all α values, of compressed plaque samples processed under different process conditions: Figure 3.5(a) for the standard condition, Figure 3.5(b) for the low extruder temperature, Figure 3.5(c) for the high extruder temperature, Figure 3.5(d) for the low screw speed, and Figure 3.5(e) for the high screw speed. All the figures indicate that the slopes of trend lines for all the α values were almost linear, and the slope decreased with the increase of α value. The slopes of these trend lines were used to calculate E_a values.

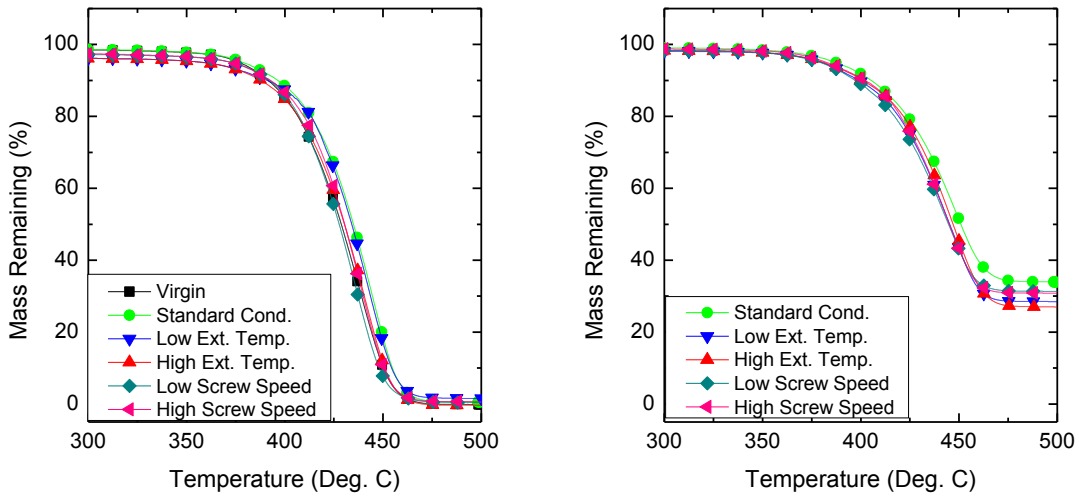

Figure 3.4 Typical TGA curves of (a) first extruder samples and (b) compressed plaque samples processed under different process conditions at a heating rate of 10 °C/min.

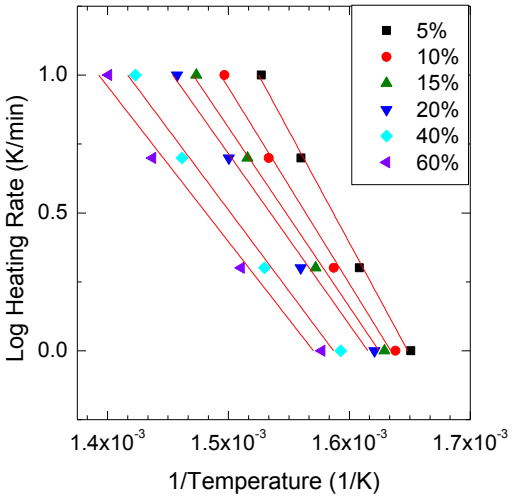
5%
10%
15%
20%
40%
60%
Log Heating Rate (K/min)
1.0
0.5
0.0
1.4x10-3
1.5x10-3
1.6x10-3
1.7x10-3
1/Temperature (1/K)

(a)

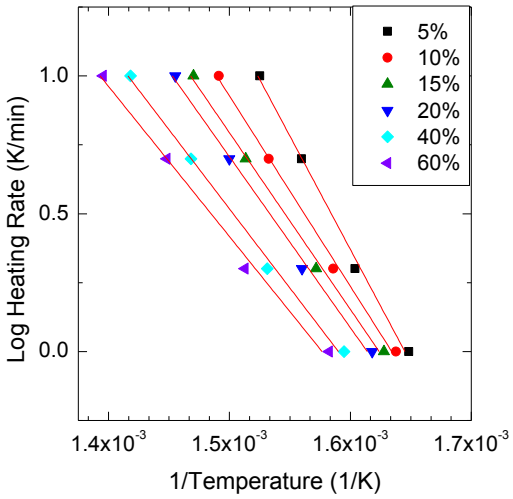
5%
10%
15%
20%
40%
60%
Log Heating Rate (K/min)
1.0
0.5
0.0
1.4x10-3
1.5x10-3
1.6x10-3
1.7x10-3
1/Temperature (1/K)

(b)

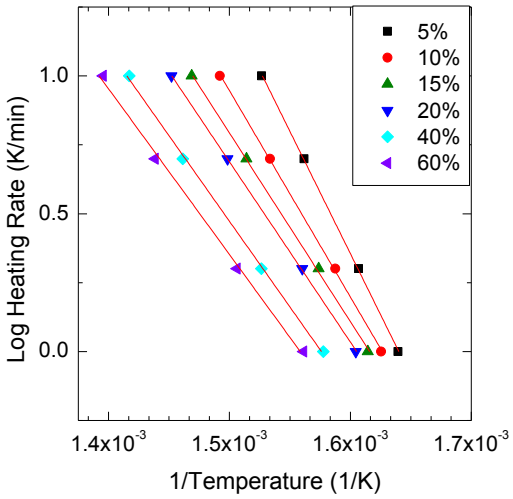
5%
10%
15%
20%
40%
60%
Log Heating Rate (K/min)
1.0
0.5
0.0
1.4x10-3
1.5x10-3
1.6x10-3
1.7x10-3
1/Temperature (1/K)

(c)

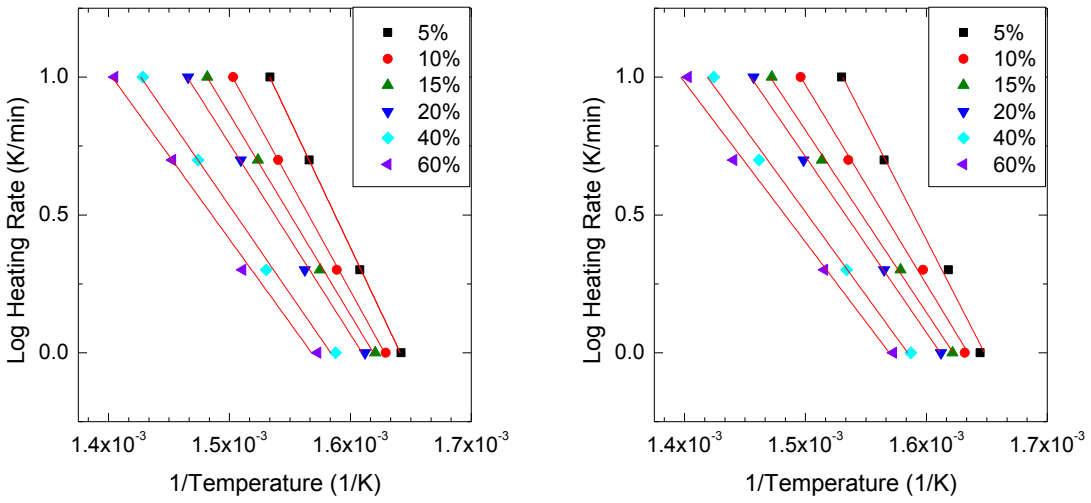

(d) (e)

Figure 3.5 Ozawa plots of compressed plaque samples process at different conversions under (a) standard condition, (b) low extruder temperature, (c) high extruder temperature, (d) low screw speed, and (e) high screw speed.

Figure 3.6 shows apparent activation energy of first extruder samples (Figure 3.6a) and compressed plaque samples (Figure 3.6b) processed under different extruder temperatures (i.e., a standard temperature of 280°C, a lower temperature of 270°C, and a higher temperature of 290°C). It can be seen from Figure 3.6 (a) and (b) that typically apparent activation energy decreased with increasing α (i.e. the percent of total decomposed material), whereas apparent activation energy increased farther along the process, that is, the virgin samples < the first extruder samples < the compressed plaque samples. As shown in Figure 3.2, the degree of discoloration increased with process progression. A possible explanation for the increase of apparent activation energy is that the content of char generated in the materials increased along the D-LFT process as a result of the increased degradation of the material. It was reported that the presence of char can

influence apparent activation energy [11], [18]. Further research into the causing mechanisms of this increase in apparent activation energy is required.

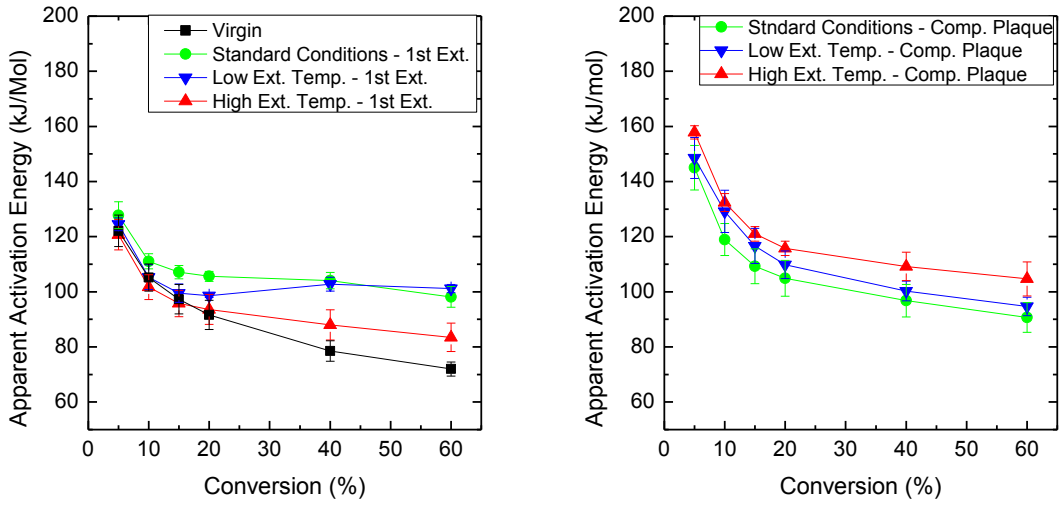

(a) (b)

Figure 3.6 Apparent activation energy throughout decomposition of (a) first extruder samples and (b) compressed plaque samples processed under different extruder temperatures.

When samples processed at different extruder temperatures are compared, the results at the end of the first extruder (Figure 3.6a) showed that the standard (medium extruder temperature) samples and the samples with the low extruder temperature had higher activation energy than the samples with the high extruder temperature for most of the conversion values. Conversely, the results after the press (Figure 3.6b) showed the samples with high extruder temperatures had slightly higher activation energy than the standard samples and the samples with the low extruder temperature for most of the conversion values. It is speculated that the increase of extruder temperature may have degraded the material with a formation of limited amounts of char at the early stage of the

D-LFT process (i.e., at the end of the first extruder) and then accelerated char formation in the material at the later stage of the D-LFT process. Further research into the causing mechanisms is required.

Figure 3.7 shows apparent activation energy of first extruder samples (Figure 3.7a) and compressed plaque samples (Figure 3.7b) processed under different screw speeds (i.e., standard screw speeds of 80 rpm for the first extruder and 50 rpm for the second extruder, lower screw speeds of 40 rpm and 25 rpm, and higher screw speeds of 161 rpm and 100 rpm). The figures suggest that the samples with the low screw speed had the highest activation energy in the range of low conversion (up to 20 %) at the end of the first extruder (Figure 3.7a) as well as for all the conversion values after the press (Figure 3.7b). The higher activation energy of the samples with the low screw speed may be due to the longer residence time at each process stage (i.e., the first extruder, second extruders, and conveyor) as shown in Table 3.2, which could have increased the amount of chars.

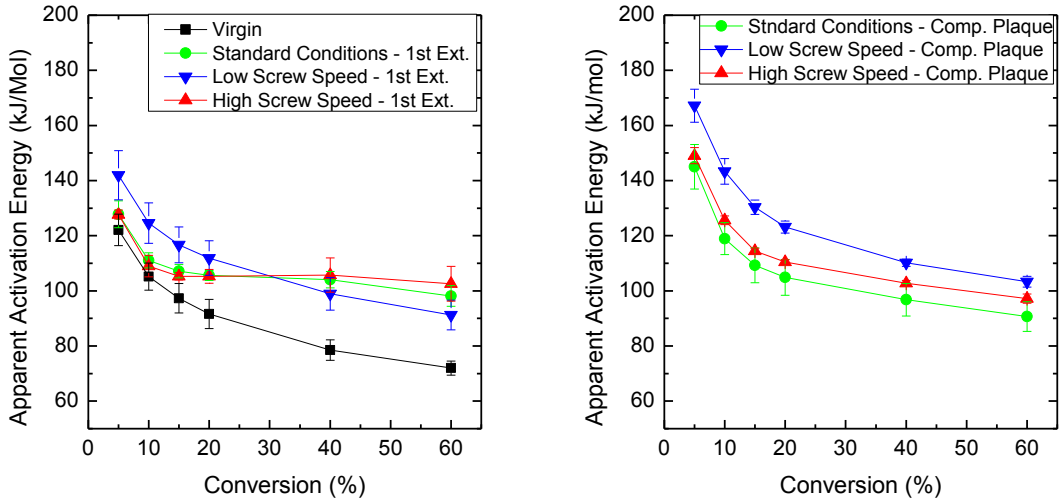

(a) (b)

Figure 3.7 Apparent activation energy throughout decomposition of (a) first extruder samples and (b) compressed plaque samples processed under different screw speeds.

3.3.4 Crystallization

3.3.4.1 Non-isothermal crystallization

Figure 3.8 shows non-isothermal DSC cooling curves of first extruder samples (Figure 3.8a) and compressed plaque samples (Figure 3.8b) processed under different processing conditions. Figure 3.9 shows subsequent heating curves of first extruder samples (Figure 3.9) and compressed plaque samples (Figure 3.9b) processed under different processing conditions. The thermal properties obtained from the DSC cooling and heating curves are summarized in Table 3.3, which includes crystallization peak temperature (T_c), enthalpy of crystallization (ΔH_c), melting peak temperatures (T_{m1}, T_{m2}), enthalpy of fusion (ΔH_m) and degree of crystallinity (X_c). The DSC cooling curves (Figure 3.8) illustrate that the crystallization peak temperature increased along the process, that is, the virgin samples < the first extruder samples < the compressed plaque samples for each

process condition. Table 3.3 suggests that the increase of extruder temperature decreased the crystallization peak temperature of the first extruder samples but had little effect on the crystallization peak temperature of the compressed plaque samples. On the other hand, the sample with the low screw speed had the lowest crystallization peak temperature after both the first extruder and press.

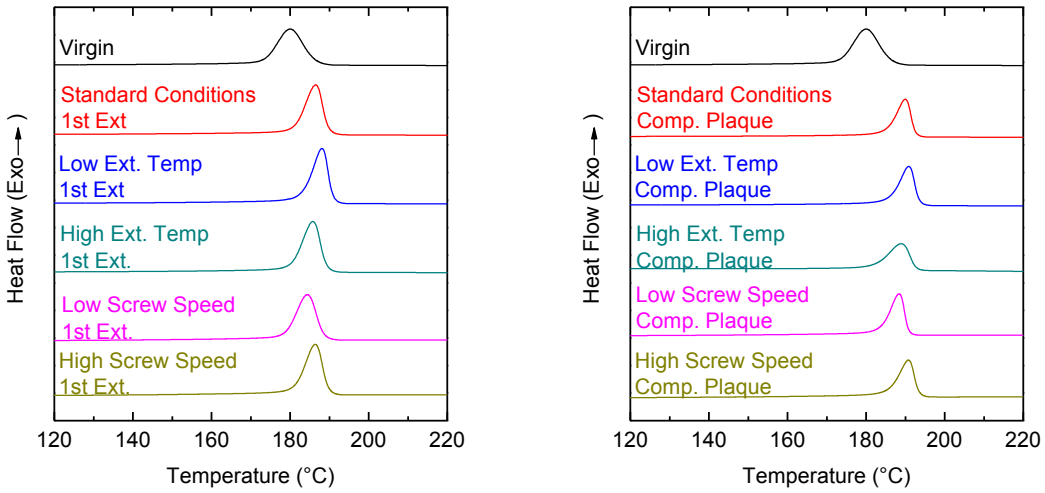

Figure 3.8 Non-isothermal DSC cooling curves of (a) first extruder samples and (b) compressed plaque samples processed under different process conditions.

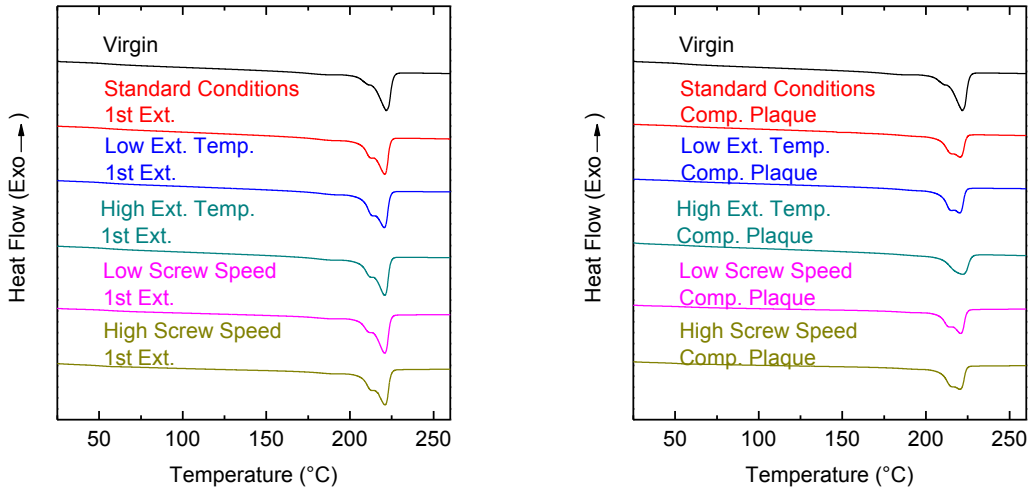

(a) (b)

Figure 3.9 Non-isothermal DSC heating curves of (a) first extruder samples and (b) compressed plaque samples processed under different process conditions.

Two melting peaks (T_{m1} and T_{m2}, where $T_{m1} < T_{m2}$) were observed on the DSC heating curves (Figure 3.9), which are associated with a difference in melting temperatures between the two phases present in the morphology (α and γ) of PA6 [19][20][21]. Table 3.3 suggests that the change of extruder temperature or screw speed had little effect on the two melting peaks and degree of crystallinity.

Table 3.3 Non-isothermal crystallization data of materials collected from the three locations within the D-LFT process. The numbers in the parenthesis are the standard deviations (n=3).

Process Location	Process Condition	T_c (°C)	ΔH_c (J/g)	T_{m1} (°C)	T_{m2} (°C)	ΔH_m (J/g)	X_c (%)
Virgin		180.3 (0.2)	61.5 (0.6)	211.1 (0.6)	221.9 (0.2)	65.7 (2.0)	28.6 (0.9)
First Extruder	Standard Condition	186.4 (0.2)	60.7 (1.2)	212.4 (0.6)	221.0 (0.1)	68.3 (1.4)	29.7 (0.6)
	Low Extruder Temperature	188.0 (0.1)	65.6 (1.4)	214.5 (0.9)	221.0 (0.3)	70.5 (2.2)	30.6 (0.9)
	High Extruder Temperature	185.7 (0.1)	65.3 (0.9)	213.5 (0.3)	221.1 (0.2)	69.4 (2.0)	30.1 (0.9)
	Low Screw Speed	184.5 (0.3)	63.1 (1.1)	213.0 (0.2)	221.0 (0.2)	67.6 (4.3)	29.4 (1.9)
	High Screw Speed	186.7 (0.5)	63.6 (0.9)	213.8 (0.3)	220.9 (0.1)	69.1 (4.0)	30.0 (1.7)
Compressed Plaque	Standard Condition	190.2 (0.2)	41.2 (0.9)	215.3 (0.2)	220.6 (0.2)	48.7 (3.8)	30.5 (2.4)
	Low Extruder Temperature	190.4 (0.4)	44.7 (1.1)	216.0 (0.6)	220.4 (0.2)	49.0 (2.8)	29.9 (1.7)
	High Extruder Temperature	190.1 (0.9)	42.6 (2.9)	215.4 (0.1)	221.0 (1.0)	46.0 (2.5)	28.1 (1.5)
	Low Screw Speed	188.0 (0.4)	43.8 (1.8)	215.1 (0.9)	221.7 (0.9)	46.7 (2.6)	28.4 (1.6)
	High Screw Speed	190.9 (0.2)	43.8 (0.5)	216.3 (0.1)	220.4 (0.1)	48.7 (1.2)	30.3 (0.8)

3.3.4.2 Isothermal crystallization

Figure 3.10 shows isothermal DSC curves of first extruder samples (Figure 3.10a) and compressed plaque samples (Figure 3.10b) processed under different process conditions. The figures suggest that crystallization speed increased after the first extruder, and further increased after the press. Figure 3.11 shows Avrami plots, i.e., plots of $\log[-\ln(1-X(T))]$ versus $\log t$, of first extruder samples (Figure 3.11a) and compressed plaque samples (Figure 3.11b) processed under different process conditions, where almost linear results were obtained from all the samples. Kinetic parameters determined by the Avrami equation are summarized in Table 3.4. The Avrami constant n decreased with glass fiber addition, which suggests that glass fiber addition had an influence on crystal nucleation mechanisms in PA6.

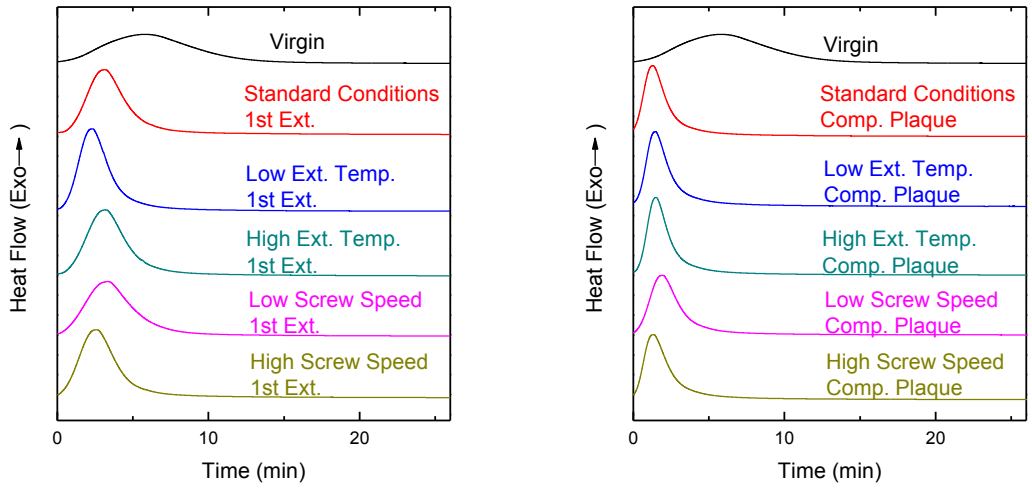

(a) (b)

Figure 3.10 Isothermal DSC crystallization curves of (a) first extruder samples and (b) compressed plaque samples processed under different process conditions.

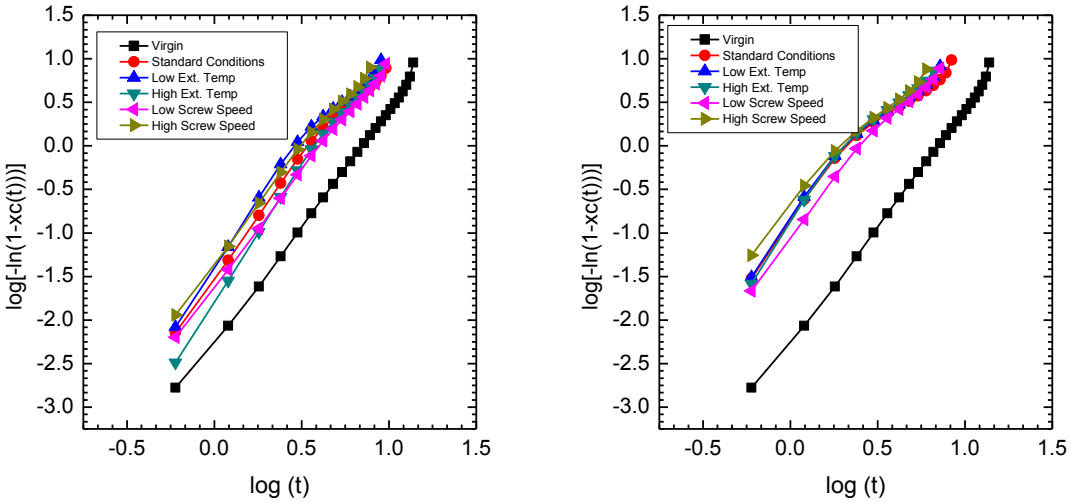

Figure 3.11 Avrami plots of (a) first extruder samples and (b) compressed plaque samples processed under different process conditions.

Table 3.4 Avrami parameters of materials collected from the D-LFT process. The numbers in the parenthesis are the standard deviations (n=3).

Process Location	Process Condition	*n*	*k* (min^{-n})
Virgin		2.69 (0.03)	$5.24x10^{-3}$ ($2.27x10^{-4}$)
First Extruder	Standard Condition	2.63 (0.15)	$2.87x10^{-2}$ ($6.25x10^{-3}$)
	Low Extruder Temperature	2.52 (0.11)	$4.36x10^{-2}$ ($8.48x10^{-3}$)
	High Extruder Temperature	2.85 (0.08)	$1.85x10^{-2}$ ($3.18x10^{-3}$)
	Low Screw Speed	2.55 (0.02)	$2.51x10^{-2}$ ($3.73x10^{-3}$)
	High Screw Speed	2.52 (0.01)	$4.17x10^{-2}$ ($1.46x10^{-3}$)
Compressed Plaque	Standard Condition	2.19 (0.12)	$1.23x10^{-1}$ ($4.94x10^{-2}$)
	Low Extruder Temperature	1.97 (0.07)	$1.63x10^{-1}$ ($1.14x10^{-2}$)
	High Extruder Temperature	2.12 (0.07)	$1.49x10^{-1}$ ($1.27x10^{-2}$)
	Low Screw Speed	2.32 (0.11)	$8.75x10^{-2}$ ($7.42x10^{-3}$)
	High Screw Speed	2.00 (0.07)	$2.13x10^{-1}$ ($3.58x10^{-3}$)

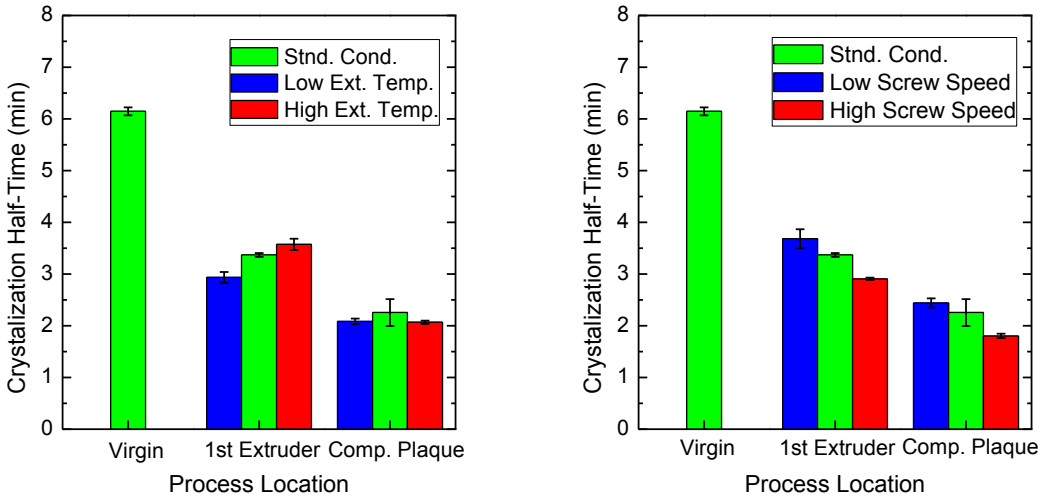

(a) (b)

Figure 3.12 Crystallization half-time of first extruder and compressed plaque samples processed under different (a) extruder temperatures and (b) screw speeds.

Figure 3.12 shows crystallization half-time from samples processed under different extruder temperatures (Figure 3.12a) and different screw speeds (Figure 3.12b). It can be seen that crystallization half-time decreases farther along the process, that is, the virgin samples > the first extruder samples > the compressed plaque samples for each process condition. Fornes and Paul [22] reported that extruded material showed faster crystallization than virgin material, and discussed reasons for this finding, namely, (i) decreased molecular weight, (ii) impurities incorporated during extrusion creating nucleation sites, and/or (iii) memory effects imposed upon the polymer during extrusion and remaining during thermal analysis. These three factors may have caused the decrease of crystallization half-time in the first extruder samples observed in this study. The further decrease of crystallization half-time in the compressed plaque samples was possibly a result of the three factors that Fornes and Paul suggested and/or the incorporation of glass fibers in the second extruder. Fibers, when introduced to a polymer, can act as

heterogeneous nucleating agents (NA) during crystallization [20], [23], [24]. If the fibers did act in such a way, they may have provided nucleation sites for crystal growth and decreased the time required for crystallization.

When samples processed at different extruder temperatures are compared (Figure 3.12a), crystallization half-time increased with increasing extruder temperature at the end of the first extruder. It is known that chain scission, branching, and cross-linking can occur in PA6 during thermal or thermo-oxidative decomposition [3]. Since the viscosity number (or molecular weight) decreased only slightly with increasing extruder temperature (Figure 3.3a), one may speculate that branching/crosslinking (i.e., interference with chain folding) had a more influence on the crystallization half-time than chain scission (i.e., chain mobility), thus increasing crystallization half-time. On the other hand, after the press, the change of extruder temperature had little effect on the crystallization half-time. The fiber incorporation may have had a more influence on the crystallization half-time than any changes of molecular structure and length of PA6. Further research into the underlying mechanisms for the extruder temperature effect is required.

When samples processed at different screw speeds are compared (Figure 3.12b), crystallization half-time increased with decreasing screw speed at the end of the first extruder. A similar explanation provided for the extruder temperature effect could be used for this phenomenon. Since the viscosity number (or molecular weight) decreased slightly with decreasing screw speed (Figure 3.3b), one may speculate that branching/crosslinking had a more influence on the crystallization half-time than chain scission, thus increasing crystallization half-time. After the press, the trend was maintained even though fibers were

added to PA6. The decrease of screw speed may have caused poor dispersion of fibers in the PA matrix (i.e., less crystal nucleation sites). Further research into the underlying mechanisms for the screw speed effect is required.

3.4 Conclusions

Effects of the extruder temperature and screw speed on the molecular weight and thermal properties of glass fiber reinforced PA6 were studied at three locations within the D-LFT process. Results from the viscosity number measurement showed that viscosity number and, by extension, molecular weight decreased with increasing extruder temperature and decreasing screw speed, which could be caused by the thermo-oxidative degradation increased under the higher extruder temperature and under the longer residence time, respectively. TGA results showed that the compressed plaque samples processed with the high extruder temperature had the highest apparent activation energy among the samples with different extruder temperatures. In addition, the compressed plaque samples processed with the low screw speed exhibited the highest apparent activation energy among the samples with different screw speeds. Non-isothermal DSC crystallization analysis revealed no substantial changes to the material's degree of crystallinity with the changes of extruder temperature or screw speed. Isothermal DSC crystallization analysis showed that the compressed plaque samples had almost constant crystallization half-time regardless of variations in the extruder temperature, but the compressed plaque samples processed with the low screw speed exhibited the longest crystallization half-time among the samples subject to different screw speeds.

References

[1] F. Henning, H. Ernst, R. Brüssel, G. Co, O. Geiger, W. Krause, and F. Institut, "LFTs for automotive applications," *Reinf. Plast.*, vol. 49, no. 2, pp. 24–33, 2005.

[2] M. Schemme, "LFT – development status and perspectives," *Reinf. Plast.*, vol. 52, no. 1, pp. 32–39, 2008.

[3] S. V. Levchik, E. D. Weil, and M. Lewin, "Thermal decomposition of aliphatic nylons," *Polym. Int.*, vol. 48, no. 7, pp. 532–557, 1999.

[4] A. G. Pedroso, L. H. I. Mei, J. A. M. Agnelli, and D. S. Rosa, "The influence of the drying process time on the final properties of recycled glass fiber reinforced polyamide 6," *Polym. Test.*, vol. 21, no. 2, pp. 229–232, 2002.

[5] R. D. Davis, J. W. Gilman, and D. L. VanderHart, "Processing degradation of polyamide 6/montmorillonite clay nanocomposites and clay organic modifier," *Polym. Degrad. Stab.*, vol. 79, no. 1, pp. 111–121, 2003.

[6] M. I. Kohan, *Nylon Plastics Handbook*. New York: Hanser Publishers, 1995.

[7] K. Pielichowski and J. Njuguna, *Thermal Degradation of Polymeric Materials*. Rapra Technology Limited, 2005.

[8] R. S. Lehrle, I. W. Parsons, and M. Rollinson, "Thermal degradation mechanisms of Nylon 6 deduced from kinetic studies by pyrolysis-g.c.," *Polym. Degrad. Stab.*, vol. 67, no. 1, pp. 21–33, 2000.

[9] C. L. Beyler and M. M. Hirschler, "Thermal Decomposition of Polymers," in *SFPE*

Handbook of Fire Protection Engineering, 4th ed., Quincy, U.S.: National Fire Protection Association, 2008, pp. 110–131.

[10] J. E. Crespo, F. Parres, M. A. Peydró, and R. Navarro, "Study of rheological, thermal, and mechanical behavior of reprocessed polyamide 6," *Polym. Eng. Sci.*, vol. 53, no. 4, pp. 679–688, Apr. 2013.

[11] X. Zuo, H. Shao, D. Zhang, Z. Hao, and J. Guo, "Effects of thermal-oxidative aging on the flammability and thermal-oxidative degradation kinetics of tris(tribromophenyl) cyanurate flame retardant PA6/LGF composites," *Polym. Degrad. Stab.*, vol. 98, no. 12, pp. 2774–2783, 2013.

[12] T. Whitfield, T. Kuboki, J. Wood, V. Ugresic, S. Sathyanarayana, and K. Dagnon, "Thermal Properties of Glass Fiber Reinforced Polyamide 6 Composites Throughout the Direct Long-Fiber Reinforced Thermoplastic," *Poloymer Eng. Sci.*, vol. Accepted, 2017.

[13] R. Sengupta, S. Sabharwal, A. K. Bhowmick, and T. K. Chaki, "Thermogravimetric studies on Polyamide-6,6 modified by electron beam irradiation and by nanofillers," *Polym. Degrad. Stab.*, vol. 91, no. 6, pp. 1311–1318, 2006.

[14] *ASTM E1641-15*. West Conshohocken, U.S.: ASTM International, 2015.

[15] B. Wunderlich, "Crystal Melting," in *Macromolecular Physics*, New York: Academic Press, 1973.

[16] M. Avrami, "Kinetics of phase change. II Transformation-time relations for random distribution of nuclei," *J. Chem. Phys.*, vol. 8, no. 2, pp. 212–224, 1940.

[17] M. Avrami, "Granulation, phase change, and microstructure kinetics of phase

change. III," *J. Chem. Phys.*, vol. 9, no. 2, pp. 177–184, 1941.

[18] K. Scully and R. Bissessur, "Decomposition kinetics of nylon-6/graphite and nylon-6/graphite oxide composites," *Thermochim. Acta*, vol. 490, no. 1–2, pp. 32–36, 2009.

[19] S. M. Aharoni, "Crystallinity and Poymorphism in the n-Nylon Family," in *n-Nylons: Their Synthesis, Structure and Properties*, Chichester, UK: John Wiley & Sons Ltd, 1997, pp. 34–70.

[20] S. Şanli, A. Durmus, and N. Ercan, "Effect of nucleating agent on the nonisothermal crystallization kinetics of glass fiber- and mineral-filled polyamide-6 composites," *J. Appl. Polym. Sci.*, vol. 125, no. SUPPL. 1, pp. E268–E281, 2012.

[21] N. Hiramatsu and S. Hirakawa, "Melting and Transformation Behavior of gamma form nylon6 under high pressure," *Polymer*, vol. 14, no. 3. pp. 165–171, 1982.

[22] T. D. Fornes and D. R. Paul, "Crystallization behavior of nylon 6 nanocomposites," *Polymer*, vol. 44, no. 14, pp. 3945–3961, 2003.

[23] J. Liang, Y. Xu, Z. Wei, P. Song, G. Chen, and W. Zhang, "Mechanical properties, crystallization and melting behaviors of carbon fiber-reinforced PA6 composites," *J. Therm. Anal. Calorim.*, vol. 115, no. 1, pp. 209–218, 2014.

[24] U. Göschel, W. Lutz, and N. C. Davidson, "The influence of a polymeric nucleating additive on the crystallisation in glass fibre reinforced polyamide 6 composites," *Compos. Sci. Technol.*, vol. 67, no. 11–12, pp. 2606–2615, 2007.

Chapter 4

4 Conclusions and Recommendations for Future Study

4.1 Conclusions

The D-LFT process offers a streamlined material processing technique and decreases the degradation of the material. To ensure product consistency and process optimization, it is imperative to understand how the process sequence affects degradation and thermal properties of the PA6 matrix, which is susceptible to degradation, during the D-LFT process. Consequently, the main objective of this study was to investigate variation in molecular weight and thermal properties of glass fiber reinforced PA6 composites at consecutive stages in the D-LFT process and under different process conditions of the tandem twin-screw extruders, which are the main components of the D-LFT process.

First, variation in molecular weight and thermal properties of the glass fiber reinforced PA6 composites throughout the D-LFT process were investigated. VN measurements, TGA, and DSC analyses were performed on samples taken from different locations along the D-LFT process. It was found that VN, which is a measure of molecular weight of the PA6 base resin, decreased throughout the processes. In contrast, TGA results suggested that apparent activation energy for decomposition increased during consecutive process stages. Non-isothermal DSC results showed that there were no significant changes to the degree of crystallization; however, isothermal DSC results indicated that later stages of the process showed a decrease in crystallization half-time, and the largest changes were observed in areas after the two extrusion portions of the process.

Second, the effects of the extruder temperature and screw speed on the molecular weight and thermal properties of glass fiber reinforced PA6 were investigated. VN measurements, TGA and DSC analyses were performed on samples taken from different locations along the D-LFT process. It was found that VN decreased with increasing extruder temperature and residence time. TGA results showed that the high temperature or low screw speed of the extruders increased apparent activation energy of the final product. Non-isothermal DSC crystallization analysis revealed no substantial changes to the material's degree of crystallinity with the variations in extruder temperature and screw speed. Isothermal DSC crystallization analysis showed that the extruder temperature had little effects on crystallization half-time of the final material, but the low screw speed of the extruders increased crystallization half-time.

In conclusion, thermo-oxidative degradation is the main degradation mechanism of the glass fiber reinforced PA6 composites during the D-LFT process. Therefore, minimizing temperature and residence time of the extruders as well as exposure time of plastificate to atmospheric conditions along the conveyer (e.g., shorten the conveyer length) is an effective way to minimize degradation of PA6. Also, the methodology developed in this study can be used to characterize variation in molecular weight and thermal properties of other composite materials at consecutive process stages within the D-LFT process.

4.2 Recommendations for Future Study

The recommended future studies are described as follows:

(1) This study showed that the trends of degree of discoloration were consistent with those of apparent activation energy of decomposition, that is, both the degree of

discoloration and apparent activation energy of decomposition increased (i) along the D-LFT process, (ii) with increasing temperature of the extruders, and (iii) with decreasing screw speed of the extruders. It is postulated that formation of char may have caused the increased degree of discoloration and apparent activation energy. It will be beneficial to study relationships among amount of char generated in the materials, degree of discoloration, and apparent activation energy, which will provide plastic manufacturers with useful information in developing PA6 tailored to the D-LFT process.

(2) This study also showed a decrease in crystallization half-time along the D-LFT process. It is speculated that the decrease was caused by the decrease in molecular weight of PA6 and/or by incorporation of fibers, which can act as heterogeneous nucleating agents. Ideification of the precise mechanisms responsible for the decreased crystallization half-time is useful for not only academia but also plastic and glass fiber manufacturers.

(3) A screw configuration of the extruders is another process parameter which could affect properties of glass fiber reinforced PA6 composites. A screw configuration can change shear stress acting on a composite melt in the extruder, thus affecting characteristics of fibers (e.g., length, dispersion, and orientation) and PA6 matrix (e.g., molecular weight, thermal decomposition, and crystallization). The study will

give useful information to select screw configurations suitable for glass fiber reinforced PA6 composites in the D-LFT process.

(4) This study characterized variation of molecular weight and thermal properties of glass fiber reinforced PA6 composites through the D-LFT process. It will be interesting to study how molecular weight and thermal properties of other composite materials change through the D-LFT process. For examples, polypropylene (less susceptible to degradation than PA6) and carbon fibers (lighter than glass fibers) can be used as the matrix and reinforcement, respectively. The study on various composite materials will give better understanding of the D-LFT process and provide equipment manufacturers with useful information to design the D-LFT process.

Appendix: Screw Configurations of Tandem Twin-Screw Extruders

The tandem twin-screw extruders used in this study consist of the first and second extruders. Both the first and the second extruders are intermeshed, co-rotating, twin-screw extruders. Each extruder has two identical, interlocking screws, which comprise a combination of four types of screw elements (i.e., a conveying element, kneading element, mixing element, and spacer element). A labeling method of a screw element is shown in Table A1. For example, the GFA-2-36-60 means a conveying element with 2 flights, a pitch of 36 mm, and a length of 60 mm. The screw configurations of the first and second extruders are shown in Table A2 and Table A3, respectively.

Table A1 Labeling Method of Screw Element

Type of Element	#	#	#
Conveying Element (GFA)	Number of flights	Pitch (mm)	Total Length (mm)
Kneading Element (KB)			
Mixing Element (GFM)			
Spacer Element (ZD)			

Table A2 Screw Configuration of the First Extruder

Polymer Intake		Polymer Melting/Mixing/Conveying																
Conveying		Kneading					Conveying		Mixing		Kneading				Conveying				
GFA-2-80-180	GFA-2-60-120	KB-2-40-60	KB-6-2-60	KB-6-2-60	KB-6-2-60	KB-6-2-60	GFA-2-60-120	GFA-2-60-120	GFM-2-60-60	GFM-2-60-60	KB-6-2-60	KB-6-2-60	KB-6-2-60	KB-6-2-60	GFA-2-60-180	GFA-2-60-120	GFA-2-60-60	GFA-2-40-60	GFA-2-40-30

Table A3 Screw Configuration of the Second Extruder

Fiber Intake						Cutting Plate	Composite Mixing/Conveying													
Conveying							Conveying with Spacers between Elements										Conveying / Mixing			
GFA-2-36-60	GFA-2-72-240	GFA-2-72-240	GFA-2-72-60	GFA-2-72-30	GFA-2-48-120		ZD-0-49.6-7.5	GFA-2-36-15	ZD-0-49.6-7.5	GFA-2-36-15	ZD-0-49.6-7.5	GFA-2-36-15	ZD-0-49.6-7.5	GFA-2-36-15	ZD-0-49.6-7.5	GFA-2-36-15	ZD-0-49.6-7.5	GFA-2-48-120	GFM-2-36-60	GFA-2-48-60	GFA-2-48-60

Curriculum Vitae

Name:	**Thomas Whitfield**
Post-secondary Education and Degrees:	The University of Western Ontario London, Ontario, Canada 2011-2015 B.E.Sc**.**
Related Work Experience	Teaching Assistant The University of Western Ontario 2015-2017
Internship	The Fraunhofer Project Center for Composites Research University of Western Ontario 2015 – 1 term

Publications:

Whitfield T, Kuboki T, Wood J, Ugresic V, Sathyanarayana S, Dagnon K. Thermal Properties of Glass Fiber Reinforced Polyamide 6 Composites Throughout the Direct Long-Fiber Reinforced Thermoplastic. Polym Eng Sci, Accepted, 2017. doi:10.1002/pen.24529.

Whitfield, T., Kuboki, T., and Wood, J. Effects of Extruder Temperature and Screw Speed on Thermal Properties of Glass Fiber Reinforced Polyamide 6 Composites Throughout the Direct Long-Fiber Reainforced Thermoplastic Process. Annual Technical Conference 2017 of Society of Plastics Engineers, Accepted, 8-10 May 2017, Anaheim, California, USA.

Fan, Y., Liu, Y. C., **Whitfield, T**., Kuboki, T., Wood, J. T., and Ugresic, V. Effects of Processing Parameters on the Thermal and Mechanical Properties of D-LFT Glass Fiber/Polyamide 6 Composites. Automotive Composites Conference and Exhibition 2016 of Society of Plastics Engineers, 7-9 September 2016, Novi, Michigan, USA.

(Poster) **Whitfield, T**., Kuboki, T., Wood, J., and Ugresic, V. Thermogravimetric Analysis of Glass Fiber Reinforced Polyamide 6. Automotive Composites Conference and Exhibition 2016 of Society of Plastics Engineers, 7-9 September 2016, Novi, Michigan, USA.

Whitfield, T., Kuboki, T., and Wood, J. Degradation of Glass Fiber Reinforced Polyamide Composites during Long Fiber Reinforced Thermoplastics Direct Extrusion Compression Moulding Process. Annual Technical Conference 2016 of Society of Plastics Engineers, Paper #252, 23-25 May 2016, Indianapolis, Indiana, USA.